LBNL-39308
UC-401
Preprint

ERNEST ORLANDO LAWRENCE
BERKELEY NATIONAL LABORATORY

Unraveling the Dissociation of Dimethyl Sulfoxide following Absorption at 193 nm

D.A. Blank, S.W. North, D. Stranges,
A.G. Suits, and Y.T. Lee
Chemical Sciences Division

August 1996
Submitted to
Journal of
Chemical Physics

DISCLAIMER

LBNL-39308
UC-401

Unraveling the Dissociation of Dimethyl Sulfoxide following Absorption at 193 nm

David A. Blank, Simon W. North, Domenico Stranges,
Arthur G. Suits, and Yuan T. Lee

Department of Chemistry
University of California, Berkeley

and

Chemical Sciences Division
Ernest Orlando Lawrence Berkeley National Laboratory
University of California
Berkeley, California 94720

August 1996

This work was supported by the Director, Office of Energy Research, Office of Basic Energy Sciences, Chemical Sciences Division, of the U.S. Department of Energy under Contract No. DE-AC03-76SF00098.

Unraveling the dissociation of di-methylsulfoxide following absorption at 193 nm.

David A. Blank, Simon W. North[a], Domenico Stranges[b], Arthur G. Suits, and Yuan T. Lee[c]
Chemical Sciences Division, Lawrence Berkeley Laboratory, University of California, Berkeley, CA 94720, USA
Department of Chemistry, University of California, Berkeley, CA 94720, USA

Abstract

We have studied the photodissociation of di-methylsulfoxide, DMSO-h_6 and DMSO-d_6, at 193 nm using the technique of photofragment translational spectroscopy with a tunable VUV product probe provided by undulator radiation on the Chemical Dynamics Beamline at the Advanced Light Source. In contrast to previous investigations we have found the dissociation to proceed via a stepwise mechanism involving multiple reaction channels. The primary dissociation, S-C bond cleavage to eliminate a methyl radical, was found to have two competing channels with distinct translational energy distributions. The translational energy distribution for the major primary dissociation channel suggests that it proceeds in a statistical manner on the ground electronic surface following internal conversion. In competition with this channel is a primary dissociation which exhibits a translational energy distribution suggestive of a dissociation on an excited electronic surface with most of the available energy being partitioned into translational and electronic degrees of freedom. Secondary decomposition of the CD_3SO intermediate was found to proceed exclusively via C-S bond cleavage, $CD_3SO \rightarrow CD_3 + SO$. However secondary decomposition of the CH_3SO intermediate was found to exhibit competition between $CH_3SO \rightarrow CH_3 + SO$ and $CH_3SO \rightarrow CH_2SO + H$. The dissociation to CH_3 and SO was the major secondary decomposition channel with the translational energy

[a] Current address: Chemistry Department, Brookhaven National Laboratory, Brookhaven, NY, 11973-5000.
[b] Permanent address: Departimento di Chimica, Universita Lasapienza Piassale a. Moro 5, 00185, Rome, Italy.
[c] Permanent address: Institute of Atomic and Molecular Science, Academica Sinica, Taipei 10764, Taiwan.

distribution indicating a barrier to recombination of >8 kcal/mol. While a minor secondary hydrogen atom elimination channel was found to play a role in secondary decomposition of CH_3SO intermediates, no analogous secondary C-D bond cleavage was detected from the CD_3SO intermediates indicating the importance of tunneling in the case of secondary C-H bond cleavage.

1. Introduction

When a molecule with two equivalent chemical bonds is excited above the threshold for dissociation of both bonds, how the rupture of the two bonds are temporally coupled becomes a salient question. For discussions of the temporal correlation of the dissociating bonds we adopt here the convenient experimental definitions of concerted and stepwise mechanisms, where concerted refers to cleavage of both bonds prior to rotation of the intermediate, and stepwise refers to cleavage of the bonds in two distinct steps with the lifetime of the intermediate exceeding its rotational period.[1] Recently the question of a concerted verses stepwise dissociation has been addressed in our laboratory for such three-body dissociations as azomethane[2] and acetone[3], where the technique of photofragment translational spectroscopy (PTS) was demonstrated to be particularly adept at resolving the dissociation dynamics. Characterization of such correlations between dissociating bonds is difficult using time resolved techniques for cases where the first step is predissocative rather than direct owing to the uncertainty in the determination of time zero.[4] Here we have continued the investigation of this class of photodissociation using PTS to study the UV dissociation of dimethylsulfoxide, DMSO. At 193 nm there is sufficient energy to break both of the C-S bonds in DMSO. The dissociation can proceed in either a concerted (reaction 1) or stepwise (reaction 2) manner:[5,6]

$$CH_3SOCH_3 \rightarrow CH_3 + SO + CH_3 \qquad \Delta H = 103 \text{ kcal/mol} \qquad (1)$$

$$CH_3SOCH_3 \rightarrow CH_3SO + CH_3 \qquad \Delta H = 51 \text{ kcal/mol} \qquad (2a)$$

$$CH_3SO \rightarrow CH_3 + SO \qquad \Delta H = 52 \text{ kcal/mol} \qquad (2b)$$

In addition to dissociation to two methyl radicals and sulfur monoxide, the following dissociation channels are also thermodynamically accessible at 193 nm:[5,6]

$$CH_3SOCH_3 \rightarrow CH_3SO + CH_3 \rightarrow CH_2SO + H + CH_3 \qquad \Delta H = 106 \text{ kcal/mol} \qquad (3)$$

$$CH_3SOCH_3 \rightarrow C_2H_6 + SO \qquad \Delta H = 13 \text{ kcal/mol} \qquad (4)$$

$$CH_3SOCH_3 \rightarrow CH_2SO + CH_4 \qquad \Delta H = 2 \text{ kcal/mol} \qquad (5)$$

The room temperature UV absorption spectrum of DMSO was recorded by Gollnick and Stracke.[7] The absorption at 188 nm was attributed to a ($\pi^* \leftarrow \pi$) transition on the SO moiety and the absorption at 205 nm to either a ($\sigma^* \leftarrow$ n) or (d $\leftarrow$ n) transition. The only published investigations of the gas phase UV photodissociation of DMSO have been reported by Chen et al. dissociating at 193 nm.[8] They used LIF (laser induced fluorescence) on both the (A-X) and (B-X) transitions to probe the the SO products, and 2+1 REMPI (resonance enhanced multiphoton ionization) to probe the methyl radical products. They found the SO vibrational distribution to be inverted, peaked at v=2. They also assigned rotational temperatures for the SO products at 750-1450 K and reported the SO quantum yield at 1.02±0.12. The results of the 2+1 REMPI measurements made on the methyl radical products found them to be internally cold with only 1.9 kcal/mol of internal energy on average in each methyl. Based on their measurements of the partitioning of the available energy the authors concluded that the dissociation of DMSO at 193 nm proceeds along a single reaction path to produce SO + $2CH_3$ in a concerted three body elimination, reaction 1. The inverted SO vibrational distribution was attributed to an elongated S-O bond length in the electronically excited DMSO. Since concerted elimination processes represent the exception for three body dissociations, the suggestion that DMSO dissociates in a concerted manner at 193 nm presents it as a particularly interesting dynamical system for investigation.

In this study we have used PTS with VUV product ionization to investigate the dissociation dynamics of DMSO-h_6 and DMSO-d_6 following absorption at 193 nm. We have observed direct evidence that the dissociation to form SO and two methyl radicals proceeds via a stepwise mechanism. Our SO photoionization measurements agree with the

internal energy measured for the SO product by Chen et al., however, our measured translational energy distributions suggest a much larger fraction of the available energy is partitioned into internal excitation of the methyl radical products than reported from the 2+1 REMPI results. In contrast to the conclusions of Chen et al. we have found the dissociation to be considerably more complex involving multiple decomposition channels. We have identified competing dissociation channels in both the primary dissociation involving C-S bond cleavage to eliminate a methyl radical as well as the secondary decomposition of the sufonyl intermediate. This study represents one of the first applications of VUV undulator radiation as a photofragment probe in PTS experiments and demonstrates this technique to be a powerful new tool for investigations in chemical dynamics.

2. Experimental

For detection of all neutral photofragments except hydrogen atoms the experiments were carried out on the Chemical Dynamics Beamline at the Advanced Light Source (ALS) at Lawrence Berkeley National Laboratory.[9] The apparatus will be described in detail in a forthcoming publication.[10,11] The design is based on an apparatus currently used in our laboratory and described elsewhere[12], with the most significant difference being the use of tunable VUV undulator radiation from the ALS for product ionization in place of electron impact ionization. A complete description of the undulator radiation at the Chemical Dynamics Beamline can be found in ref. 11. The light is continuously tunable from 8-50 eV with a bandwidth of 2.5% providing an average of $5x10^{15}$ photons/second at the fundamental energy and substaintial power in the higher harmonics. The undulator radiation is passed through a harmonic filter which consists of a gas cell containing 30 torr of noble gas. For undulator radiation at energies below the I.P. for the noble gas the filter is transparent, however for undulator radiation above the I.P. of the noble gas the filter provides a $>10^4$ suppression of the light. By selecting a noble gas with an I.P. between the fundamental and the second harmonic energy of the undulator radiation the higher order hamonics from the undulator are efficiently filtered from the

VUV beam. The undulator radiation is then focused to 150 x 200 micrometers at the point of intersection with the dissociation products.

A continuous molecular beam of either DMSO-h_6 or DMSO-d_6, <1% in He, was generated by bubbling 40-60 torr of He through a room temperature liquid sample and expanding the resulting mixture through a 0.25 mm stainless steel nozzle into a source chamber maintained at $1x10^{-4}$ torr. The nozzle was heated to 80°C to inhibit cluster formation and the resulting molecular beam typically had a r.m.s. velocity of 1080 m/s with FWHM of 15%. After being skimmed twice the molecular beam was intersected at 90° by the output of a Lambda Physik LPX200 excimer laser operating on the ArF transition (193.3 nm) with laser fluence ranging 1-500 mJ/cm^2. The molecular beam was rotatable about the axis of the dissociation laser, with the dissociation laser and detector axis fixed mutually perpendicular. Neutral photofragments which recoiled out of the molecular beam traveled 15.1 cm where they were photoionized by the undulator radiation, mass selected with a quadrupole mass filter, and counted as a function of time using a Daly ion counter.[13]

For detection of hydrogen atoms a similar apparatus was used with modifications designed to increase sensitivity for m/e 1 photofragments which have been discussed previously.[14] In this configuration a pulsed molecular beam of <1% DMSO-h_6 in He, the dissociation laser, and the detector axis are all fixed mutually perpendicular. The dissociation laser intersects the unskimmed molecular beam 5 mm above the pulsed nozzle exit. Neutral photofragments which recoil at 90° from the molecular beam pass through two defining apertures and travel 37.0 cm where they are ionized by electron impact, mass selected, and counted as a function of time in the same manner as described above.

Center of mass translational energy distributions , $P(E_T)$'s, for the neutral photofragments were obtained from the time of flight spectra, TOF, using the forward convolution technique.[12,15]

DMSO-h_6, 99%, and DMSO-d_6, 99.9% isotopic purity, were obtained from Aldrich and used without further purification.

3. Results

For all of the TOF spectra presented the open circles represent the data, the dashed lines are single channel contributions to the forward convolution fit, and the solid line is the overall fit to the data.

3.1 DMSO-d_6

The TOF spectra for m/e 66 (CD_3SO^+) at source angles of 12° and 22.5° are shown in figure 1. Each spectrum is the result of $2x10^6$ laser shots with the undulator radiation set at 11.0 eV. Not only do these spectra directly identify CD_3SO as a primary dissociation product, reaction 2a, but the spectra suggest that there is more than one dissociation channel resulting in CD_3SO photoproducts. The spectrum at 12° exhibits a clear shoulder ~80 μsec and the spectrum has been fitted with two separate contributions. The presence of the fast contribution is confirmed in the 22.5° spectrum. The c.m. translational energy distribution for each of the two contributions are shown in figure 2. The slow channel , fig. 2a, is peaked around 8 kcal/mol and has a tail which extends beyond 30 kcal/mol. The fast channel, fig. 2b, is peaked at 26 kcal/mol and extends to 42 kcal/mol. Additional evidence for two channels leading to CD_3SO can be seen in figure 3, the TOF spectrum for m/e 64 (CD_2SO^+) at 12°, which was taken under the same photoionization conditions as the m/e 66 spectra. Different dissociation channels leading to CD_3SO products will demonstrate different dissociative ionization patterns as a result of the distinct internal energy distributions in the CD_3SO products. Figure 3 has been fitted with the $P(E_T)$s in figure 2 and it is clear that while the slow feature is still evident with dissociative ionization slightly favoring the translationally slower, and therefore internally warmer, fragments, the fast feature is not observed at the CD_2SO mass. The failure to detect any of the fast channel at m/e 64 demonstrates that the CD_3SO fragments from that channel are vibrationally much cooler than the slow channel with an internal energy distribution distinct from the slow dissociation channel.

The TOF spectra for m/e 18 (CD_3^+) at source angles of 20°, 35°, and 50° are shown in figure 4 and were taken with the undulator radiation set at 12.0 eV and without the use of the harmonic filter. The spectra have been fitted with three contributions. The

fastest contribution is fitted with the $P(E_T)$ for the fast channel observed at m/e 66, figure 2b, confirming the fast methyl as the momentum matched dissociation partner of the fast CD_3SO fragment. The remaining two contributions are the broad contribution peaked ~80 μsec which are the methyl products from the slow primary dissociation, reaction 2a, and the contribution peaked ~55 μsec representing methyl products which result from secondary decomposition of those primary CD_3SO fragments produced with sufficient internal energy to undergo secondary dissociation, reaction 2b. The $P(E_T)$ for the slow primary dissociation is shown in figure 5a. It is peaked near zero with an exponential decrease extending beyond 30 kcal/mol. Since methyl radical products do not undergo secondary decomposition, the $P(E_T)$ in figure 5a represents the complete $P(E_T)$ for the slow primary dissociation. Figure 6 shows the $P(E_T)$ from figure 5a along with the $P(E_T)$ from figure 2a which is the $P(E_T)$ for the slow primary CD_3SO products which survive. The primary $P(E_T)$ for CD_3SO intermediates which undergo secondary decomposition is the difference between figures 5a and 2a which is the crossed-hatched region in figure 6. For a discussion of the truncation in the primary $P(E_T)$ for the surviving CD_3SO photofragments see section 4.2. The $P(E_T)$ for the secondary decomposition of CD_3SO intermediates, reaction 2b, produced in the slow primary dissociation is shown in figure 5b. It is peaked at 8 kcal/mol and extends to 32 kcal/mol.

TOF spectra for m/e 48 (SO^+) at source angles of 25°, 40°, and 50° are shown in figure 7 and were taken under the same photoionization conditions as the m/e 18 spectra. The fit to the TOF consists predominantly of the signal from the secondary decomposition of the CD_3SO intermediates produced in the slow primary dissociation channel. There is a small contibution to the m/e 48 TOF spectra from dissociative ionization of CD_3SO intermediates which is peaked ~130 μsec and is most evident in the 25° spectrum. As mentioned above for the secondary CD_3 products, the primary $P(E_T)$ for CD_3SO intermediates which undergo secondary decomposition is represented by the difference between figure 5a and 2a, see figure 6. The m/e 48 (SO^+) spectra were fitted using the secondary $P(E_T)$ in figure 5b confirming the secondary methyl contribution in the m/e 18 TOF spectra to be the momentum matched partner of the SO. Although the fits to the secondary decomposition of the CD_3SO intermediates at m/e 18 (CD_3^+) and m/e 48 (SO^+)

were not sensitive to the precise shape of the secondary angular distribution, the fits did require that the secondary angular distribution maintain forward/backward symmetry.

Branching Ratios. The branching ratios are depicted in figure 8. The branching ratios were obtained from the fitting ratios of the three contributions to the m/e 18 (CD_3^+) TOF spectra. We therefore assumed that under the experimental photoionization conditions the photoionization cross-section for the methyl radical products was independent of their internal energy. All kinematic considerations are accounted for in the fitting procedure. The ratio of the three channels used to obtain the best fit to the m/e 18 spectra was 19(fast primary) :52(slow primary) :29(secondary). This yields a ratio of 27:73 for the fast primary dissociation channel to the slow primary dissociation channel. With the secondary dissociation proceeding exclusively from the slow primary dissociation, the fitting ratios indicate that 56% of the CD_3SO fragments produced in the slow primary dissociation undergo secondary decomposition. The best fits to the CD_3SO spectra, m/e 66, were obtained with a ratio of 44(fast):56(slow). This ratio of the fast primary CD_3SO products to the surviving slow primary CD_3SO intermediates is consistent with the measured ratios for the m/e 18 spectra. With 56% of the slow primary channel undergoing secondary decomposition the result is a ratio of 45:55 for the fast primary channel to the surviving slow secondary CD_3SO products which is consistent with the fitting ratio for the m/e 66 TOF spectra. The majority of the error in the branching ratios obtained in this fashion results from the ability to adjust the fitting ratios while maintaining a reasonable fit to all of the TOF data. We estimate this error to be <10%.

3.2 DMSO-h_6

We were not able to observe TOF spectra for m/e 63 (CH_3SO^+). The inability to directly detect the CH_3SO intermediate is the result of a number of experimental factors. As will be shown, in comparison with the CD_3SO intermediates, a greater percentage of the CH_3SO intermediates produced in the slow primary dissociation undergo secondary decomposition. In addition, the fast primary dissociation is less prevalent in the case of DMSO-h_6. Although this accounts for a reduction of ~30% in the yield of CH_3SO intermediates in the dissociation, the most substantial reduction in signal results from the

necessity to increase the resolution of the quadrupole mass filter to permit sufficient discrimination between m/e 62 and m/e 63. The increased resolution is concomitant with a severe reduction in transmission of the quadrupole. The low signal at m/e 66 (CD_3SO^+) from the the CD_3SO intermediate was likely the result of preferential photodissociation rather than photoionization, and the additional reductions in signal for the CH_3SO rendered it unobservable under the experimental conditions.

Although we were not able to detect any signal at m/e 63 (CH_3SO^+), we observed a substantial signal at m/e 62. The TOF spectrum for m/e 62 (CH_2SO^+) at a source angle of 15 degrees is shown in figure 9. The spectrum was taken with the undulator radiation set at 12 eV without the harmonic filter. The signal at m/e 62 can be attributed to either dissociative ionization of CH_3SO intermediates or to secondary decomposition of the CH_3SO intermediates involving hydrogen atom elimination, reaction 3. Direct evidence for reaction 3 is shown in figure 10, the TOF spectrum for m/e 1 (H^+). The fit to the m/e 1 TOF spectrum contains three contributions. The slow contribution, peaked at 110 μsec, is the contribution from dissociatively ionized methyl radical products scattered to 90°. The contribution at early times, peaked at 30 μsec, exhibits a near quadratic dependence on the dissociation laser fluence and has been fitted as a two photon dissociation with the first photon yielding methyl radical products and the second photon dissociating the methyl radicals to methylene and hydrogen atoms. The $P(E_T)$ for methyl radical photodissociation at 193 nm has been previously determined in this laboratory[14] and was used in the fitting for the secondary step in the two photon dissociation. The remaining middle feature, peaked at 50 μsec, had a linear dependence on the laser power and was fitted assuming a stepwise mechanism for reaction 3. The translational energy distributions for the primary, $CH_3SOCH_3 \rightarrow CH_3 + SOCH_3$, and the secondary dissociation, $SOCH_3 \rightarrow SOCH_2 + H$, are shown in figure 11. The $P(E_T)$s in figure 11 were also used to fit the TOF spectrum for m/e 62 in figure 9 providing strong evidence that the m/e 62 TOF signal is the result of reaction 3. The primary $P(E_T)$ is peaked at 6 kcal/mol and exponentially declines beyond 30 kcal/mol, and the secondary $P(E_T)$ is peaked at 4 kcal/mol and extends to 18 kcal/mol.

TOF spectra for m/e 15 (CH_3^+) at source angles of 20° and 35° are shown in figure 12. The undulator radiation was set at 11 eV and the harmonic filter was used with

argon.[11] The fitting is analogous to the m/e 18 (CD_3^+) spectra described above with the same three individual contributions. Owing to reasons discussed above, we were not able to observe spectra for the CH_3SO fragment and we have therefore assumed the $P(E_T)$ in figure 2b from the fast primary dissociation channel of DMSO-d_6 in fitting the fast contribution peaked ~30 μsec. The remaining two contributions are the slow primary dissociation, the slowest and broadest contribution peaked around 70 μsec, and subsequent secondary decomposition of the CH_3SO intermediate, reaction 2b, peaked ~40 μsec. The $P(E_T)$ for fitting the slow primary dissociation, reaction 2a, is shown in figure 13a and is identical to the analogous $P(E_T)$ for the deuterated case, figure 5a. The $P(E_T)$ used to fit the secondary decomposition, reaction 2b, is shown in figure13b. The TOF spectra for the momentum matched secondary SO fragments, m/e 48 (SO^+), at source angles of 20°, 30°, and 45° are shown in figure 14. The dominant contribution is from decomposition of the CH_3SO intermediates, reaction 2b, fitted with the secondary $P(E_T)$ in figure 13b. At 20° and 30° there is a small contribution on the slow side from dissociative ionization of CH_3SO photofragments. Although the secondary $P(E_T)$ is very similar to the analogous $P(E_T)$ for the deuterated dissociation, figure 5b, it is slightly broader. This difference in the shape results from competition in the secondary dissociation with hydrogen atom elimination in DMSO-h_6. As with the fits to the DMSO-d_6 data, the secondary angular distribution was not sensitive to the exact shape of the distribution, however the fits did require that forward/backward symmetry be maintained.

Photoionization spectrum of the SO product: Figure 15 shows the relative intensity of the TOF signal at m/e 48 and a source angle of 20° as a function of the photoionization energy from 8.25 eV to 11.0 eV. For this measurement, in addition to the rare gas harmonic filter, the undulator radiation passed through a 3 mm thick MgF_2 window to further reduce background from residual high energy photons above the transmission cutoff for MgF_2 of about 11.2 eV. The undulator radiation was roughly gaussian in shape with a FWHM of 0.5 eV. From figure 15 the ionization onset for the SO products is ~9.5 eV. Taking into consideration the bandwidth of the undulator radiation, this corresponds to an onset of ~9.8 eV. The vertical I.P. for sulfur monoxide is 10.32 ±

0.02 eV.[17] The difference between the ionization onset for the SO product and the vertical I.P. reflects an internal energy content in the SO of 0.50 ± 0.15 eV.

Branching Ratios. The branching ratios are depicted in figure 8. The ratio between the fast primary channel, slow primary channel, and secondary C-S bond cleavage was obtained from the fits to the m/e 15 (CH_3^+) spectra. The best fit to the data resulted from a ratio of 11:54:35 respectively indicating 65% of the CH_3SO intermediates produced in the slow primary step undergo secondary decomposition. The error in the ratios between the contributions in the m/e 15 fits is analogous to the case of DMSO-d_6, <10%. In order to estimate the percentage of the secondary hydrogen elimination, reaction 3, we must compare the signal intensity of the m/e 62 and m/e 15 TOF spectra. Since there is no current information on the photoionization cross-section for CH_2SO at 12 eV we make the assumption that the photoionization cross-sections of CH_3 at 11.0 eV and CH_2SO at 12.0 eV are equal and we estimate the contribution of reaction 3 at <5% overall.

4. Discussion

4.1 Primary dissociation, reaction 2a. Detection of the CD_3SO product at m/e 66, figure 1, provides strong evidence that the dissociation to sulfur monoxide and two methyl radicals coes not exclusively proceed via a three body process. The TOF spectrum for m/e 66 at 12° in figure 1 exhibits a shoulder on the fast side suggesting two contributions to the spectrum, a fast contribution peaked at 80 μsec and a slow broad contribution peaked at 100 μsec. The existence of two separate contributions is confirmed by the differing dissociative ionization at m/e 64 (CD_2SO^+), figure 3, indicating the production of two different m/e 66 photoproducts with distinct vibrational energy distributions. As discussed above we were not able to detect the CH_3SO photoproducts due to experimental limitations, see section 3.2, however the fits to the TOF spectra at m/e 15 confirm the analogous fast and slow primary dissociations in the case of DMSO-h_6.

4.1.1 Fast primary dissociation. The $P(E_T)$ for the fast primary dissociation, reaction 2a, shown in figure 2b is peaked at 24 kcal/mol and extends to a maximum of 42 ± 5 kcal/mol. Assuming the maximum in the $P(E_T)$ reflects the production of vibrationally/rotationally cold products and neglecting the internal energy of the DMSO

reactant[18], the maximum in the $P(E_T)$ represents the available energy following photodissociation at 193 nm (148 kcal/mol). Given an available energy of of 42 ± 5 kcal/mol and using $\Delta H_f(DMSO)$ = -31.4 kcal/mol and $\Delta H_f(CH_3)$ = 34.8 kcal/mol[5] the result is $\Delta H_f(CH_3SO)$ = 40 ± 5 kcal/mol. Comparison of this value to the value obtained from group additivity of $\Delta H_f(CH_3SO)$ = -15 kcal/mol[6] suggests that the fast primary dissociation might result in the production of an excited electronic state of CH_3SO which lies ~55 kcal/mol above the ground electronic state. The lack of dissociative ionization of the fast m/e 66 (CD_3SO^+) product to m/e 64 (CD_2SO^+) as compared with the slow primary dissociation, see figures 1 and 2, indicates the fast CD_3SO product is vibrationally much cooler than the slow CD_3SO product. This also indicates that the electronically excited CD_3SO products must undergo radiative relaxation during the ~30 μsec collisionless flight to the detector since nonradiative relaxation would result in vibrational excitation which is not evident in the dissociative ionization at m/e 64 (CD_2SO^+). The large fraction of available energy partitioned intc translation, $\langle E_{trans} \rangle$ = 26 kcal/mol, and the fact that the distribution is peaked at 24 kcal/mol suggests either direct dissociation on a repulsive electronic surface or electronic predissociation on a surface with a large barrier to recombination.

From the absorption spectrum of Gollnick and Stracke[7] the dominant absorption at 193 nm should be a ($\pi^* \leftarrow \pi$) transition on the SO moiety. The fast primary dissociation may then be the result of electronic predissociation involving a repulsive electronic surface. Comparison of TOF spectra taken at m/e 18 (CD_3^+) and 35° with the dissociation laser polarized at -45°, 0°, 45°, and 90° with respect to the detector axis demonstrated no difference in the overall TOF spectra. Assuming an isotropic angular distribution for the slow primary dissociation, a reasonable assumption for a statistical dissociation on the ground electronic surface, see section 4.1.2, no change in the relative intensity of the fast to slow contributions in the TOF with polarization suggests a near isotropic angular distribution for the fast primary dissociation. A first order approximation of the dipole moment for a ($\pi^* \leftarrow \pi$) transition within C_{2v} symmetry places the dipole moment in the plane of the molecule along the S=O bond. Based on a ground state CSC bond angle of 96.4° (ref. 7) the angle between the dipole and the C-S bond is 48.2° which leads to an

anisotropy parameter[19] of $\beta = 0.34$ in the limit of a prompt dissociation. While in the excited state the CSC bond angle might be expected to increase, this would only lead to a decrease in the limiting value of β. In addition, any rotational averaging of the reactant molecule prior to dissociation will also serve to decrease the value of β. Our data for m/e 18 at various laser polarization angles is not sufficient to distinguish within this small range of values for β, $0>\beta>0.3$. Therefore our measurement of an angular distribution for the fast primary channel which appears nearly isotropic in the laboratory frame is consistent with electronic predissociation from the π^* surface on even a very rapid timescale owing to our lack of sensitivity of the degree to which the distribution is anisotropic.

4.1.2 Slow primary dissociation. The $P(E_T)$ for the slow primary dissociation, reaction 2a, is shown in figures 5a and 13a for DMSO-d_6 and DMSO-h_6 respectively. Within experimental error figure 5a and 13a are the same. Note that the $P(E_T)$ in figure 2a determined from the slow m/e 66 (CD_3SO^+) photoproducts differs from figures 5a and 13a on the low energy side. As will be discussed below, a significant fraction of the slow CD_3SO products undergo secondary decomposition and therefore the $P(E_T)$ in figure 2a represents only those CD_3SO photofragments which survive. The $P(E_T)$ in figures 5a and 13a were determined from the methyl radical product which does not secondarily decompose and therefore represents the complete $P(E_T)$ for the slow primary dissociation.

The $P(E_T)$ for the slow primary dissociation, figure 5a or 13a, is peaked at 2 kcal/mol and decreases exponentially out beyond 30 kcal/mol. Translational energy distributions of this type, peaked near zero with an exponentially decreasing tail, are characteristic of a statistical dissociations on the ground electronic surface involving little or no recombination barrier. From the endothermicity of the primary C-S bond cleavage, $D_o(CH_3\text{-}SOCH_3) = 51$ kcal/mol[5,6], the available energy following absorption at 193 nm (148 kcal/mol) is 97 kcal/mol. In the case of a statistical translational energy distribution the extremely low probabililty for formation of products with a translational energy release greater than half of the available energy severely limits our sensitivity to the $P(E_T)$ above 50 kcal/mol. For comparison, figure 16 shows a prior distribution for dissociation of a rotationally cold molecule into two polyatomic fragments of 4 and 6 atoms each within the rigid rotor, harmonic oscillator, and spherical top approximations and given 97 kcal/mol of

available energy.[20] The prior distribution represents a completely statistical prediction against which the experimentally determined distribution may be compared. From figure 16 it is clear that the measured $P(E_T)$, dashed line in figure 16, is in excellent agreement with the prior translational energy distribution, solid line in figure 16. Our results indicate that in the case of the slow primary dissociation the initial electronic excitation is followed by internal conversion to the ground electronic surface and C-S bond cleavage to produce two open shell molecules with little or no barrier to recombination.

4.2 Secondary decomposition of the sulfonyl intermediate, CD_3SO/CH_3SO. Following the primary dissociation, reaction 2a, the sufonyl intermediates containing sufficient internal energy will undergo secondary decomposition. We found no evidence for the secondary dissociation of intermediates produced in the fast primary dissociation. The fast primary dissociation, see section 4.1.1, results in the production of electronically excited sulfonyl radicals with a substantial fraction of the available energy appearing in translation. The predominant partioning of the available energy into translational and electronic degrees of freedom and the lack of dissociative ionization of the fast m/e 66 (CD_3SO^+) photoproduct at m/e 64 (CD_2SO^+) are consistent with the persistence of the sulfonyl radicals produced in the fast primary dissociation.

In contrast with the fast primary dissociation, sulfonyl intermediates produced in the slow primary dissociation should contain ample internal energy to undergo secondary dissociation. As discussed in section 4.1.2, the slow primary dissociation is a statistical, near prior, dissociation on the ground electronic surface. Figure 6 shows the overall slow primary $P(E_T)$ with the $P(E_T)$ for the surviving CD_3SO fragments overlaid. The distributions are the same above ~20 kcal/mol but at lower translational energy, and thus higher internal energy of the products, the distribution for the surviving CD_3SO fragments begins to fall off. The difference between the two distributions, the cross-hatched area in figure 6, represents the CH_3SO/CD_3SO fragments which undergo secondary decomposition. The gradual decline in the $P(E_T)$ for the surviving CD_3SO fragments toward lower translational energy reflects the broad internal energy distribution of the methyl partner fragment. In contrast with atomic elimination where a given translational energy release reflects a well defined internal energy in the polyatomic partner fragment

which results in an abrupt truncation of the $P(E_T)$ for the surviving polyatomic fragment[21], the broad internal energy distribution in the methyl partner fragment allows a broad distribution of internal energy in the CD_3SO fragments for a given translational energy release yielding a gradual truncation of the $P(E_T)$.

The onset of the truncation in the $P(E_T)$ for surviving CD_3SO photofragments occurs at the point where internally cold methyl radicals are produced along with sulfonyl radicals with internal energy equal to the height of the barrier to secondary sulfonyl radical decomposition. The recombination barrier for secondary C-S bond cleavage is > 8 kcal/mol, see section 4.2.1. Adding the recombination barrier to the C-S bond energy for the sulfonyl radical of ~52 kcal/mol the barrier to secondary C-S bond cleavage is ~60 kcal/mol. The onset of the truncation in the primary $P(E_T)$ should therefore occur at ~37 kcal/mol since the available energy following primary C-S bond cleavage is ~97 kcal/mol. With the onset of the truncation reflecting production of internally cold methyl radicals, the portion of the $P(E_T)$ measured for the surviving sulfonyl intermediates below ~37 kcal/mol directly reflects the internal energy distribution of methyl radicals produced with surviving sulfonyl radicals. As can be seen in figure 2a the $P(E_T)$ lies almost entirely below 37 kcal/mol.

Using the prior model, figure 16, to predict the internal exitation in the sulfonyl intermediate following the slow primary dissociation, $\langle E_{int}(CD_3SO/CH_3SO)\rangle_{prior} = 58$ kcal/mol with the distribution extending beyond 90 kcal/mol. Both cleavage of the C-S bond, reaction 2b, and cleavage of the C-H/C-D bond, reaction 3, are, therefore, thermodynamically accessible pathways for secondary decomposition of the sulfonyl intermediate.

4.2.1 Secondary decomposition of the CD_3SO/CH_3SO intermediate: C-S bond cleavage. Cleavage of the C-S bond, reaction 2b, was the dominant secondary dissociation channel for the CH_3SO intermediates, and the only secondary decomposition pathway detected for the CD_3SO intermediates. As discussed above in section 4.2 the difference between the the overall $P(E_T)$ for the slow primary dissociation and the $P(E_T)$ for surviving sulfonyl intermediates, the cross-hatched area in figure 6, represents primary $P(E_T)$ for the CH_3SO/CD_3SO fragments which undergo secondary decomposition. In figure 6 the

difference between the two distributions represents 55% of the total distribution, consistent with 56±10% secondary decomposition determined from the CD_3 TOF spectra fitting ratios. For reasons discussed in section 3.2 we were unable to directly detect the surviving CH_3SO photofragments, however in the fitting we assumed the primary $P(E_T)$ for CH_3SO intermediates which secondarily dissociate to be the same as that for the CD_3SO photofragments. From the fitting ratios in the CH_3 TOF spectra we find that 64±10% of the CH_3SO intermediates undergo secondary decomposition. This corresponds to a quantum yield for the SO of 0.6±0.1 compared to the quantum yield reported by Chen et al. for SO of 1.02±0.12. [8]

The $P(E_T)$ determined for secondary C-S bond cleavage is shown in figure 5b for CD_3SO and figure 13b for CH_3SO. The distributions are very similar, however the $P(E_T)$ for CH_3SO decomposition is slightly broader and a little flatter at the top of the distribution. This difference is likely the result of competing C-H bond cleavage in the case of CH_3SO decomposition which is discussed in the following section. In addition, stiffer modes in the CH_3 product as compared to the CD_3 product might result in less vibrational excitation of the CH_3 product and, therefore, a slightly faster $P(E_T)$ for the CH_3SO decomposition. The translational energy distributions, figure 5b and 13b, are peaked at ~8 kcal/mol suggesting a barrier to recombination of >8 kcal/mol. If one considers a dissociation model for simple bond rupture over an exit barrier where the available energy is partitioned in an impulsive fashion up to the height of the barrier to recombination and statistically above the barrier[3] then the maximum probability in the translational energy distribution will reflect the barrier to recombination. The success of this model for different chemical systems with widely differing available energies has shown that the barrier to recombination is predominantly responsible for energy partitioned into translation even when the available energy greatly exceeds the barrier height.[4] The limiting case results if all the potential energy of the recombination barrier appears in translation. Since it is possible for some portion of that potential energy to evolve into internal degrees of freedom as the dissociation proceeds, our measured maximum in the $P(E_T)$ represents a lower limit to the recombination barrier. In the case of both the deuterated and nondeuterated DMSO the fits to the data were not sensitive to the exact shape of the

secondary angular distribution, however the fits did require that the secondary angular distribution maintain forward/backward symmetry, demonstrating rotational averaging of the CD_3SO intermediate prior to secondary C-S bond dissociation and providing direct evidence that reaction 2 proceeds via a stepwise mechanism.[23] In the case of a concerted three body elimination we would have measured a strong correlation between the primary and secondary recoil velocity vectors.[2]

Our measurement of the SO internal energy found 11.5±3.5 kcal/mol on average which agrees well with the more accurate measurement of Chen et al. who found an average of 8.9 kcal/mol with the vibrational distribution peaked at v=2.[8] From our results we conclude that SO products result from a stepwise dissociation, reaction 2, with a statistical primary dissociation followed by secondary decompostition over a recombination barrier of > 8 kcal/mol. This suggests that the dynamical partitioning of available energy into SO internal degrees of freedom results from strong exit channel effects in the secondary decomposition of the sulfonyl intermediate.

From the measured branching ratios we find a quantum yield for CH_3/CD_3 of 1.4±0.1. This is in excellent agreement with recent diode absorption gain measurements made by Rudolph and coworkers who determined a quantum yield of 1.4±0.1 for CD_3 from the dissociation of DMSO-d_6 at 193 nm.[22] In addition, Rudolph and coworkers determined the fraction of nacent methyl radical products formed in the vibrational ground state. Their measurements suggest an internal energy content of the CD_3 products in excess of the REMPI measurments of Chen et al.[8] and below the internal energy content which had been previously determined for CD_3 products in the dissociation of acetone-d_6 at 193 nm.[24] For comparison we can make a qualitative esitimate of the vibrational energy in the methyl radical products based on our overall picture of the dissociation of DMSO-d_6 at 193 nm. The fast primary dissociation accounts for 19% of the total methyl radiacal yield. Using the soft fragment impulsive model[4] with 42 kcal/mol of available energy, see section 4.1.1, we estimate $\langle E_{int}(CH_3/CD_3)\rangle \sim 4$ kcal/mol for the fast primary dissociation. For the slow primary dissociation, which accounts for 52% of the total methyl radical yield, we use the prior model, see section 4.1.2, to estimate $\langle E_{int}(CH_3/CD_3)\rangle \sim 32$ kcal/mol. The remaining 29% of the methyl radical products are the result of secondary

decomposition of sulfonyl intermediates. As discussed earlier in this section, the forward barrier to C-S bond cleavage in the sulfonyl radical intermediates is ~60 kcal/mol. For sulfonyl radicals produced in the slow primary dissociation we can again use the prior model as an estimate of the internal energy distribution, see figure 16. Truncating the distribution below 60 kcal/mol to represent only those sulfonyl intermediates which undergo secondary decomposition yields $<CH_3SO/CD_3SO>_{int}$ ~ 67 kcal/mol. With $D_o(CH_3\text{-}SO)$ ~ 52 kcal/mol[5,6], $<E_T>$ = 11 kcal/mol for secondary C-S bond cleavage, and $<E_{int}(SO)>$ ~9 kcal/mol[8] suggests very little energy remaining in internal energy of the methyl radical. Based on these estimations, overall the methyl radical products will contain ~17 kcal/mol of internal energy each on average. While we aknowledge the severity of the approximations made in this estimation it clearly suggests a larger internal energy content in the methyl products than the REMPI measurements of Chen et al.

4.2.2 Secondary decomposition of the CH_3SO intermediate: C-H bond cleavage. The primary and secondary translational energy distributions for reaction 3 which were determined from the fitting of the m/e 62 (CH_2SO^+) and m/e 1 (H^+) TOF spectra are shown in figure 11. Our inability to detect any evidence of C-D bond cleavage in the CD_3SO intermediates suggests that secondary C-H bond cleavage involves tunneling through the dissociation barrier. The secondary $P(E_T)$, figure 11b, is peaked at ~ 4 kcal/mol. Since the C-H bond cleavage appears to involve tunneling, the barrier to recombination should be slightly higher than the 4 kcal/mol reflected by the maximum in the $P(E_T)$. This places the barrier to secondary dissociation for reaction 2b and reaction 3 in very close proximity of one another, see figure 17. Figure 11a shows the $P(E_T)$ for the primary C-H bond cleavage and although it is similar to the overall slow primary $P(E_T)$, figure 13a, it is missing a portion of the low energy side. In contrast, the primary $P(E_T)$ for sulfonyl intermediates which undergo secondary C-S bond cleavage, the region cross-hatched in figure 6, is missing the high energy side in comparison to the overall slow primary $P(E_T)$. This indicates that CH_3SO intermediates that go on to break a C-H bond are internally cooler, and therefore translationally warmer, on average compared with those that break the C-S bond. The resulting overall picture for the secondary decomposition of the CH_3SO intermediates shows that the fraction of CH_3SO

intermediates with substantial internal energy above the barriers to secondary dissociation result almost exclusively in C-S bond cleavage. However, a small portion of the CH_3SO intermediates with internal energy near the dissociation barriers are able to competitively break the C-H bond with tunneling playing an important role.

5. Conclusion

We have used the technique of photofragment translational spectroscopy with VUV synchrotron radiation for product ionization to investigate the photodissociation of DMSO-h_6 and DMSO-d_6 at 193 nm. A picture of the overall dissociation including all of the observed dissociation channels and the estimated barriers is shown in figure 17. In contradiction to previous studies we found direct evidence that dissociation to sulfur monoxide and two methyl radicals occurs via a stepwise dissociation on the ground electronic surface. In addition we also found competing dissociation channels in both the primary and secondary steps. A small fraction of the primary dissociation results in a very large translation energy release and appears to involve dissociation on an excited electronic surface to form methyl radical and an electronically excited state of the sulfonyl radical. With the majority of the available energy partitioned into electronic and translational degrees of freedom the sulfonyl radicals from the fast primary dissociation lack sufficient internal energy to undergo secondary decomposition. The majority of the primary dissociation occurs following an initial ($\pi^* \leftarrow \pi$) excitation and internal conversion to the ground electronic surface. Primary C-S bond cleavage then proceeds over little or no barrier resulting in a statistical, near prior, partitioning of the available energy. In the case of DMSO-d_6 all of the CD_3SO intermediates with sufficient internal energy to overcome the barrier to C-S bond cleavage, 56% of the $SOCD_3$ produced in the slow primary dissociation, dissociate via reaction 2b. In the case of DMSO-h_6 those sulfonyl intermediates with internal energy well above the barrier to secondary C-S bond cleavage go on to dissociate via reaction 2b, however a small fraction of CH_3SO intermediates with internal energy near the dissociation barriers are able to break the C-H bond with tunneling playing a significant role.

Acknowledgments

The authors would like to thank R. N. Rudolph for providing a preprint of the results of the diode absorption gain experiments. The authors would like to thank Dr. G. E. Hall for many helpful discussions. This work was supported by the Director, Office of Energy Research, Office of Basic Energy Sciences, Chemical Sciences Division of the U. S. Department of Energy under contract No. DE-AC03-76SF0009. The experiments were conducted at the Advanced Light Source, Lawrence Berkeley National Laboratory which is supported by the same source.

References

[1] C. E. M. Strauss and P. L. Houston, *J. Phys. Chem.*, **94**, 8751 (1990).

[2] S. W. North, C. A. Longfellow, and Y. T. Lee, *J. Chem. Phys.*, **99**, 4423 (1993).

[3] S. W. North, D. A. Blank, J. D. Gezelter, C. A. Longfellow, and Y. T. Lee, *J. Chem. Phys.*, **102**, 4447 (1995).

[4] S. W. North, Ph.D. thesis, University of California, Berkeley, 1995.

[5] The heat of formation for DMSO was taken from *Phys. Chem. Ref. Data*, **17**, (1988) Suppl. No. 1.
The heats of formation for SO, CH_3, H, C_2H_6, and CH_4 were taken from Handbook of Chemistry and Physics, CRC Press, 1995.

[6] The heat of fromation for CH_3SO and CH_2SO were based on group additivity from S. W. Benson, *Chem. Rev.*, **78**, 23 (1978).

[7] K. Gollnick and H. U. Stracke, *Pure Appl. Chem.*, **33**, 217 (1973).

[8] X. Chen, F. Asmar, H. Wang, and B. R. Weiner, *J. Phys. Chem.*, **95**, 6415 (1991).
X. Chen, H. Wang, B. R. Weiner, M. Hawley, and H. H. Nelson, *J. Phys. Chem.*, **97**, 12269 (1993).

[9] M. Koike, P. A. Heimann, A. H. Kung, T. Namioka, R. DiGennaro, B. Gee, N. Yu, *Nuclear Instruments and Methods in Physics Research A*, **347**, 282 (1994).
P. A. Heimann, M. Koike, C. W. Hsu, M. Evans, C. Y. Ng, D. Blank, X. M. Yang, C. Flaim, A. G. Suits, and Y. T. Lee, *SPIE Proceedings 2856* (1996).

[10] X. Yang, D. A. Blank, J. Lin, P. A. Heimann, A. M. Wodtke, A. Suits, and Y. T. Lee, *to pe published.*

[11] A. G. Suits, P. Heimann, X. Yang, M. Evans, C. Hsu, K. Lu, and Y. T. Lee, *Rev. Sci. Instrum.*, **66**, 4841 (1995).

[12] A. M. Wodtke and Y. T. Lee, *J. Phys. Chem.*, **89**, 4744 (1985).

[13] Y. T. Lee, J. D. McDonald, P. R. LeBreton, and D. R. Herschback, *Rev. Sci. Instrum.*, **40**, 1402 (1969); N. R. Daly, *ibid*, **31**, 264 (1960).

[14] S. W. North, D. A. Blank, P. M. Chu, and Y. T. Lee, *J. Chem. Phys.*, **102**, 791 (1995).

[15] X. Zhao, Ph.D. Thesis, University of California, Berkeley (1989).

[17] Handbook of Chemistry and Physics, CRC Press, 1995.

[18] DMSO at 298 K contains ~2.3 kcal/mol of vibrational energy on average and should experience substantial cooling following supersonic expansion.

[19] R. N. Zare. *Mol. Photochem.*, **4**, 1 (1972).

[20] R. D. Levine and R. B. Bernstein, *Acc. Chem. Res.*, 7, 393 (1974).
J. T. Muckerman, *J. Phys. Chem.*, **93**, 179 (1989).

[21] T. K. Minton, P. Felder, R. J. Brudzynski, and Y. T. Lee, *J. Chem. Phys.*, **81**, 1759 (1984).
S. W. North, D. A. Blank, and Y. T. Lee, *Chem. Phys. Lett.*, **222**, 38 (1994).

[22] R. N. Rudolph, S. N. North, G. E. Hall, T. J. Sears, *manuscript in preparation.*

[23] P. M. Kroger and S. J. Riley, *J. Chem. Phys.*, **67**, 4483 (1977).
P. M. Kroger and S. J. Riley, *J. Chem. Phys.*, **70**, 3863 (1979).

[24] G. E. Hall, D. Vanden Bout, and T. J. Sears, *J. Chem. Phys.*, **94**, 4182 (1991).

Figure Captions

Figure 1: TOF spectra for m/e 66 (CD_3SO^+) at source angles of 12° and 22.5°. The forward convolution fit contains two contributions representing the fast and slow channels for reaction 2a and fit with the $P(E_T)$s in figure 2.

Figure 2: (a) c.m. translational energy distribution used to fit the slow contribution in the m/e 66 (CD_3SO^+) TOF spectra, figure 1. (b) c.m. translational energy distribution used to fit the fast contribution in the m/e 66 (CD_3SO^+) TOF spectra, figure 1.

Figure 3: TOF spectrum for m/e 64 (CD_2SO^+) at a source angle of 12°. The fit shown is from the two $P(E_T)$s in figure 2 with the same fitting ratio used to fit the m/e 66 (CD_3SO^+) spectra in figure 1. Note absence of the fast feature in the expermental data.

Figure 4: TOF spectra for m/e 18 (CD_3^+) at source angles of 20°, 35°, and 50°. The forward convolution fit has three componenets. The fastest component, peaked ~40 μsec, is fit with the $P(E_T)$ in figure 2b and represents the fast channel for reaction 2a. The slowest and broadest component, peaked ~80 μsec, is fitted with the $P(E_T)$ in figure 5a and represents the slow channel for reaction 2a. The middle contribution, peaked ~55 μsec, is fitted with the secondary $P(E_T)$ in figure 5b and represents products from reaction 2b.

Figure 5: (a) Primary c.m. translation energy distribution used to fit the slowest contribution to the m/e 18 (CD_3^+) TOF spectra in figure 4, slow channel for reaction 2a. (b) Secondary c.m. translation energy distribution for reaction 2b used to fit the middle contribution to the m/e 18 (CD_3^+) TOF spectra in figure 4 and the dominant contribution to the m/e 48 (SO^+) TOF spectra in figure 7.

Figure 6: The c.m. translational energy distribution from figure 2a overlayed on the c.m. translation energy distribution from figure 5a. The area with the cross-hatches is the difference between figure 5a and figure 2a and represents the primary c.m. translation energy distribution for sulfonyl intermediates which undergo secondary C-S bond cleavage.

Figure 7: TOF spectra for m/e 48 (SO^+) from dissociation of DMSO-d_6 at source angles of 25°, 40°, and 50°. The dominant contribution to the forward convolution fit is the result of reaction 2b and is fitted with the $P(E_T)$ in figure 5b. The small contribution to the fit at 25°, peaked ~125 μsec, is from dissociative ionization of CD_3SO photoproducts.

Figure 8: Branching ratios for the dissociation of DMSO-d_6 and DMSO-h_6 at 193 nm. Determination of the values is discussed in the text. The error in the values is estimated to be <10%.

Figure 9: TOF spectrum for m/e 62 (CH_2SO^+) at a source angle of 15°. The forward convolution fit is from the primary and secondary $P(E_T)$s in figure 10a and 10b according to reaction 3.

Figure 10: TOF spectrum for m/e 1 (H^+) with the detector, molecular beam, and dissociation laser mutually perpendicular. The forward convolution fit contains three contributions. The fastest contribution, peaked ~40 μsec, is a two photon dissociation involving C-S bond cleavage followed by secondary photodissociation of the methyl radical products. The slowest contribution, peaked ~105 μsec, is from dissociative ionization of methyl radical products. The middle contribution, peaked ~60 μsec is fit with the primary and secondary $P(E_T)$s in figures 10a and 10b according to reaction 3.

Figure 11: (a) Primary c.m. translation energy distribution used to fit the m/e 62 (CH_2SO^+) TOF spectrum in figure 8 and the middle contribution to the m/e 1 (H^+) TOF spectrum in figure 9, reaction 3. (b) Secondary c.m. translation energy distribution for reaction 3 used to fit the m/e 62 (CH_2SO^+) TOF spectrum in figure 8 and the middle contribution to the m/e 1 (H^+) TOF spectrum in figure 9.

Figure 12: TOF spectra for m/e 15 (CH_3^+) at source angles of 20° and 35°. The forward convolution fit has three componenets. The fastest component, peaked ~40 μsec, is fit with the $P(E_T)$ in figure 2b and represents the fast channel for reaction 2a. The slowest and broadest component, peaked ~75 μsec, is fit with the $P(E_T)$ in figure 12a and represents the slow channel for reaction 2a. The middle contribution, peaked ~45 μsec, is fit with the secondary $P(E_T)$ in figure 12b and represents products from reaction 2b.

Figure 13: (a) Primary c.m. translation energy distribution used to fit the slowest contribution to the m/e 15 (CH_3^+) TOF spectra in figure 11, slow channel for reaction 2a. (b) Secondary c.m. translation energy distribution for reaction 2b used to fit the middle contribution to the m/e 15 (CH_3^+) TOF spectra in figure 11 and the dominant contribution to the m/e 48 (SO^+) TOF spectra in figure 13.

Figure 14: TOF spectra for m/e 48 (SO^+) from dissociation of DMSO-h_6 at source angles of 20°, 30°, and 45°. The dominant contribution to the forward convolution fit is the result of reaction 2b and is fit with the $P(E_T)$ in figure 12b. The small contribution to the fit at 20°, peaked ~125 μsec, is from dissociative ionization of CH_3SO photoproducts.

Figure 15: Photoionization spectrum for m/e 48 (SO^+) photofragments from DMSO-h_6 at a source angle of 20° for undulator radiation energies of 8.25-10.75 eV. The VUV had a roughly gaussian shape with FWHM of 0.5 eV.

Figure 16: Calculated prior distributions for dissociation of a rotationally cold reactant into 4 and 6 atom fragments within the rigid rotor, harmonic oscillator, and spherical top approximations with 70 kcal/mol of available energy. The solid line is the calculated translational energy distribution. The dotted line is the internal energy distribution of the 4 atom product. The dot-dash-dot line is the internal energy distribution of the 6 atom product. The dashed line is the primary $P(E_T)$ for the slow channel of reaction 2a from figures 5a and 12a.

Figure 17: A summary of the dissociation channels which we observed for DMSO following absorption at 193 nm. Thermodynamic values are from ref. 5 and ref. 6 and estimations for the energy of S1, T1, and S2 are from ref. 7. Relative contributions of each channel are shown in figure 8.

figure 1

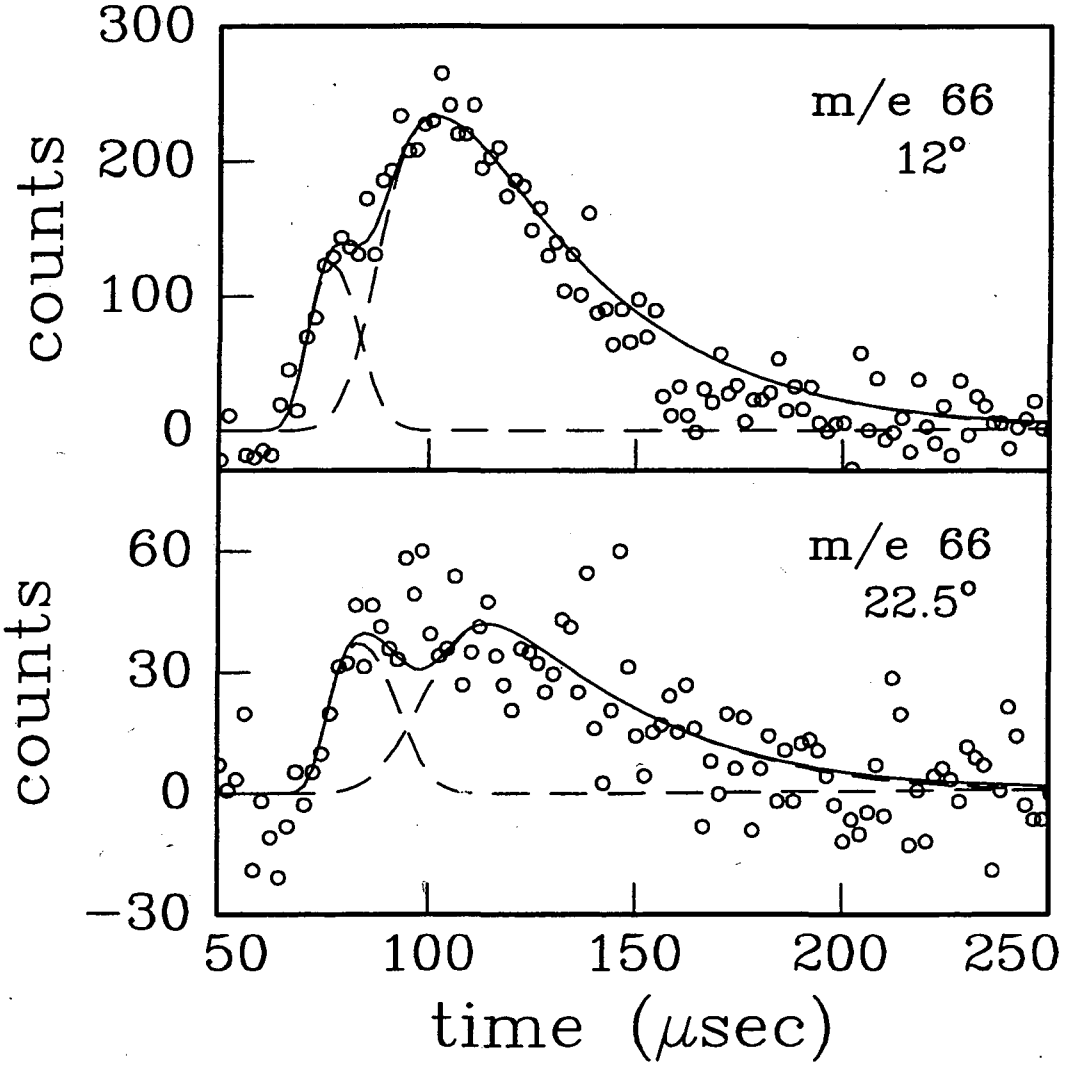
300
200
100
0
counts
m/e 66
12°
60
30
0
−30
counts
m/e 66
22.5°
50
100
150
200
250
time (μsec)

figure 2

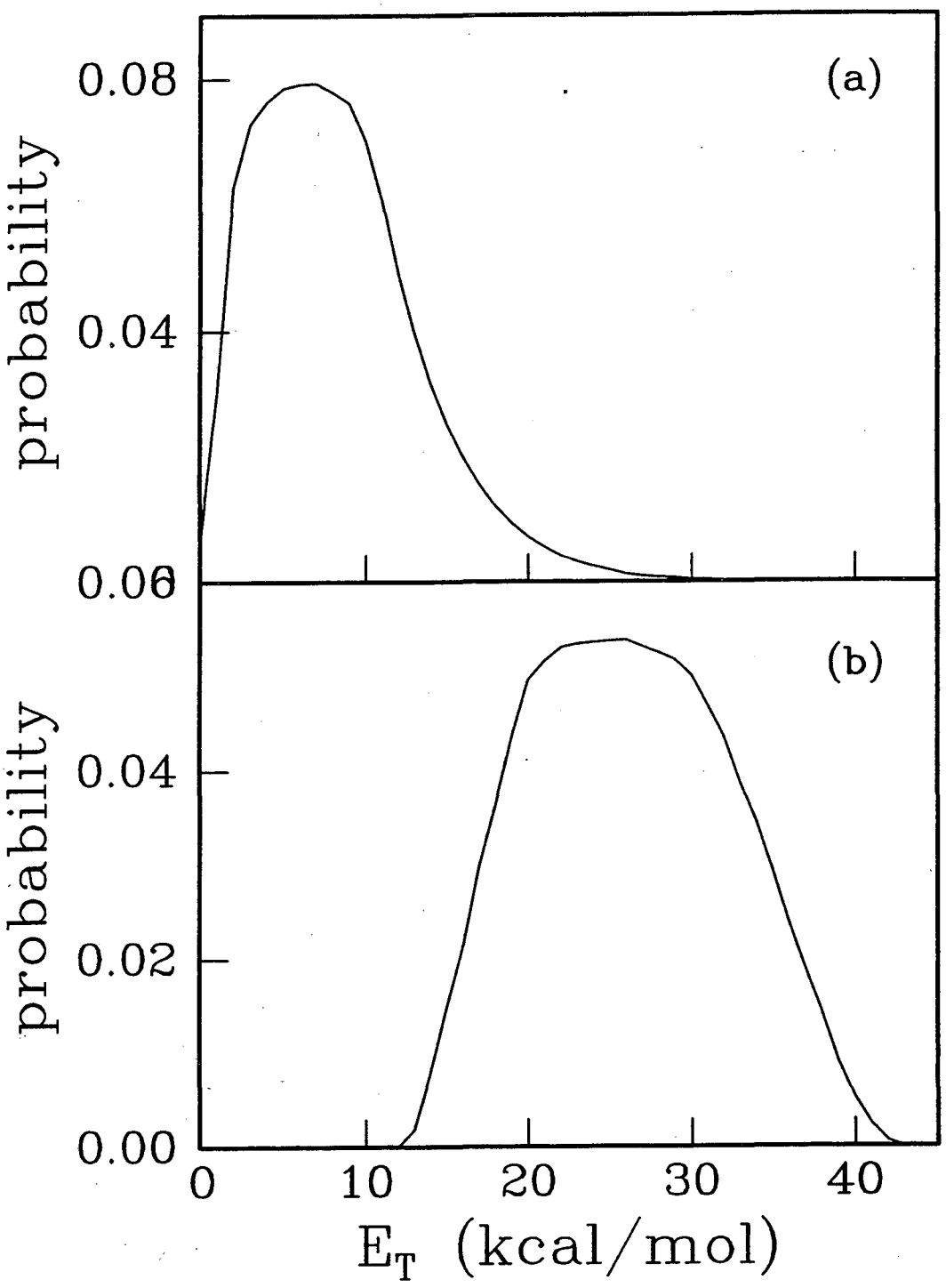
0.08
0.04
0.00
probability
(a)
0.04
0.02
0.00
probability
(b)
0
10
20
30
40
E_T (kcal/mol)

figure 3

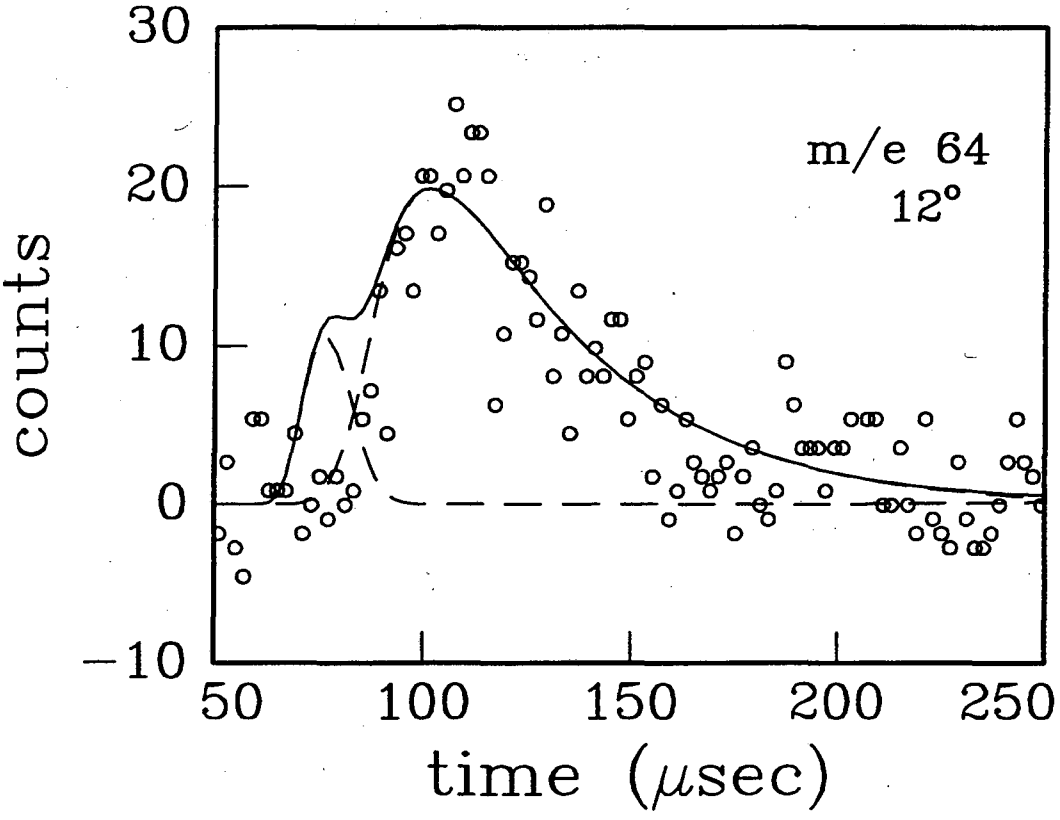

figure 4

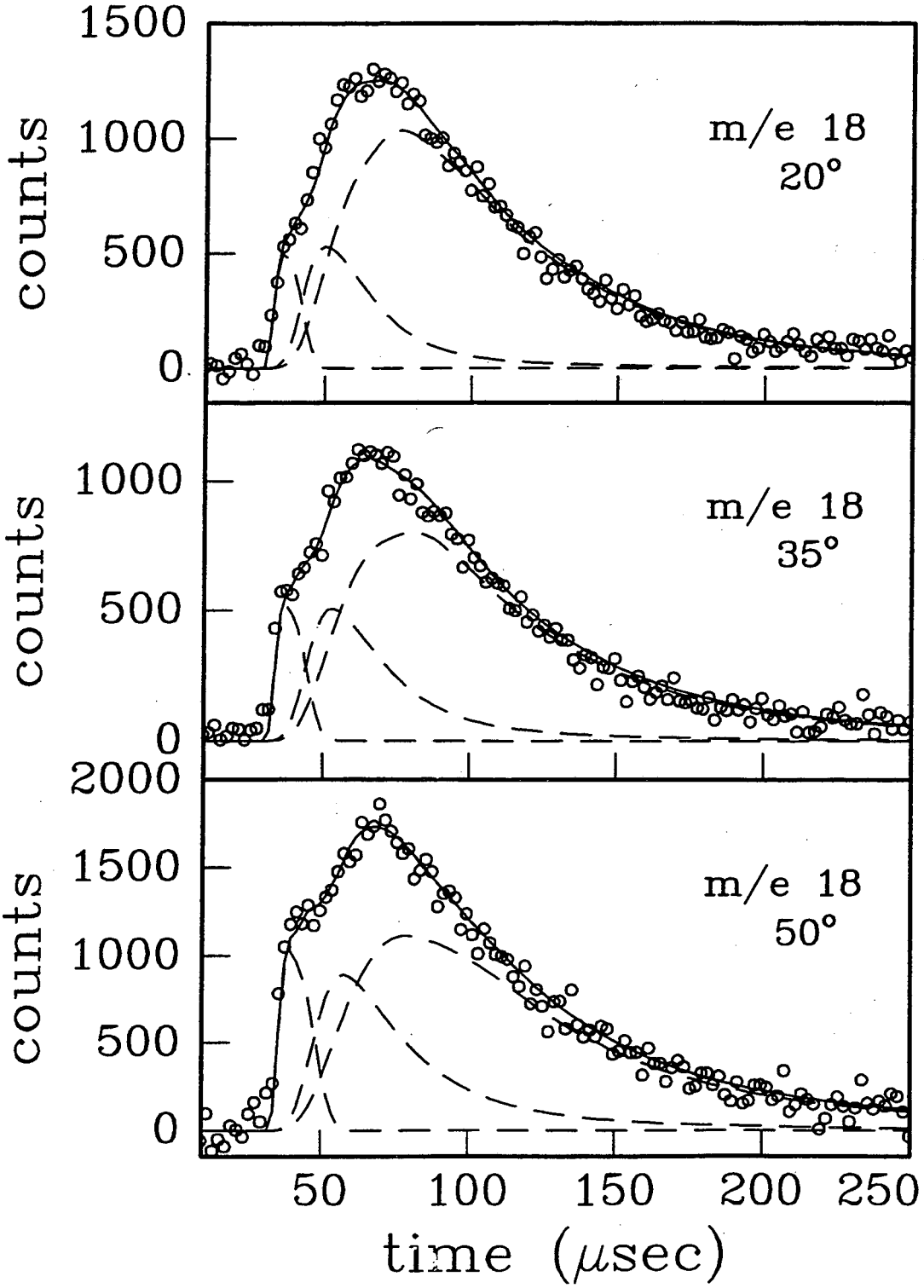
1500
1000
500
0
counts
m/e 18
20°
1000
500
0
counts
m/e 18
35°
2000
1500
1000
500
0
counts
m/e 18
50°
50
100
150
200
250
time (μsec)

figure 5

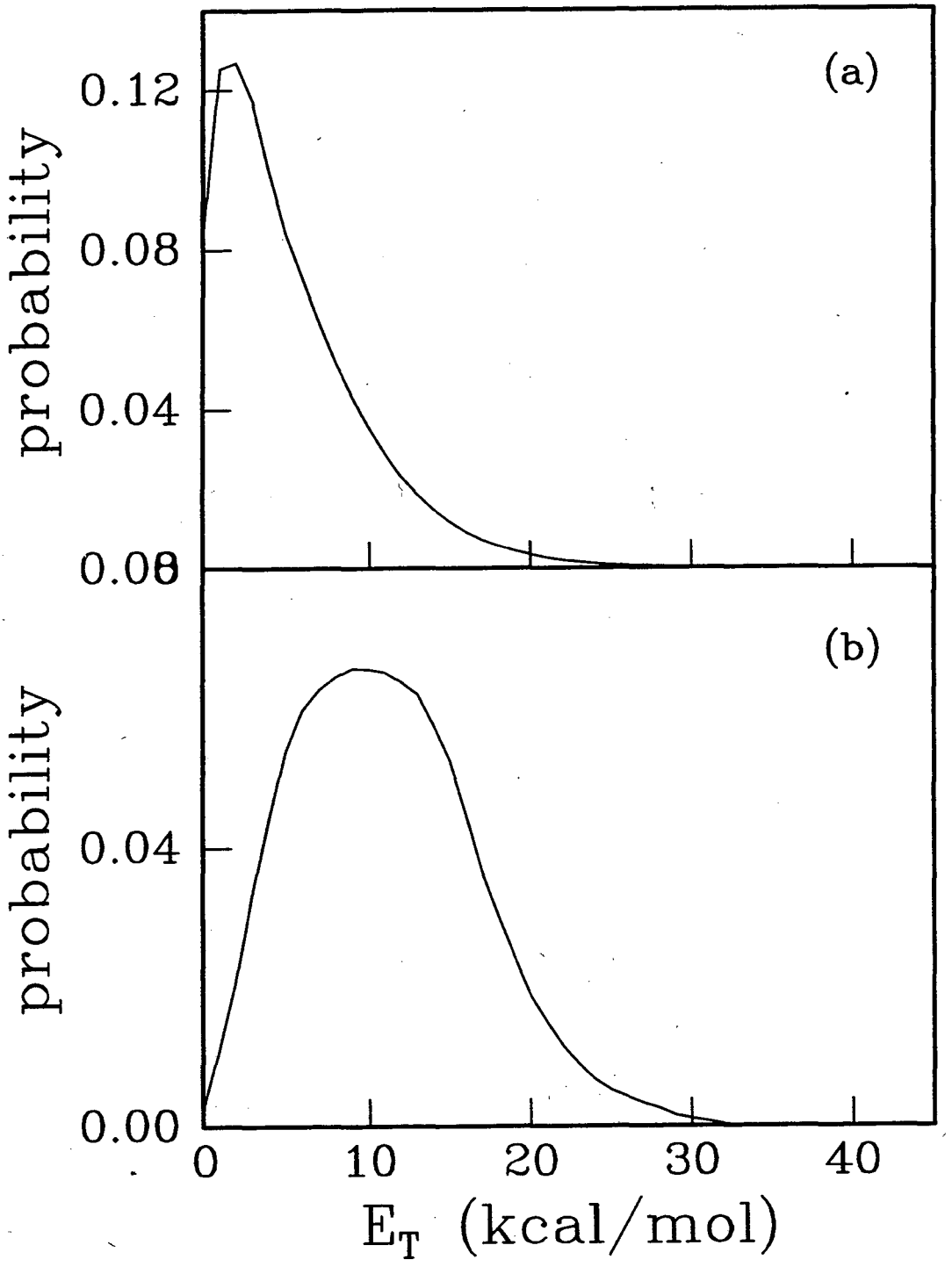
(a)
0.12
0.08
0.04
0.00
probability
(b)
0.04
0.00
probability
0
10
20
30
40
E_T (kcal/mol)

figure 6

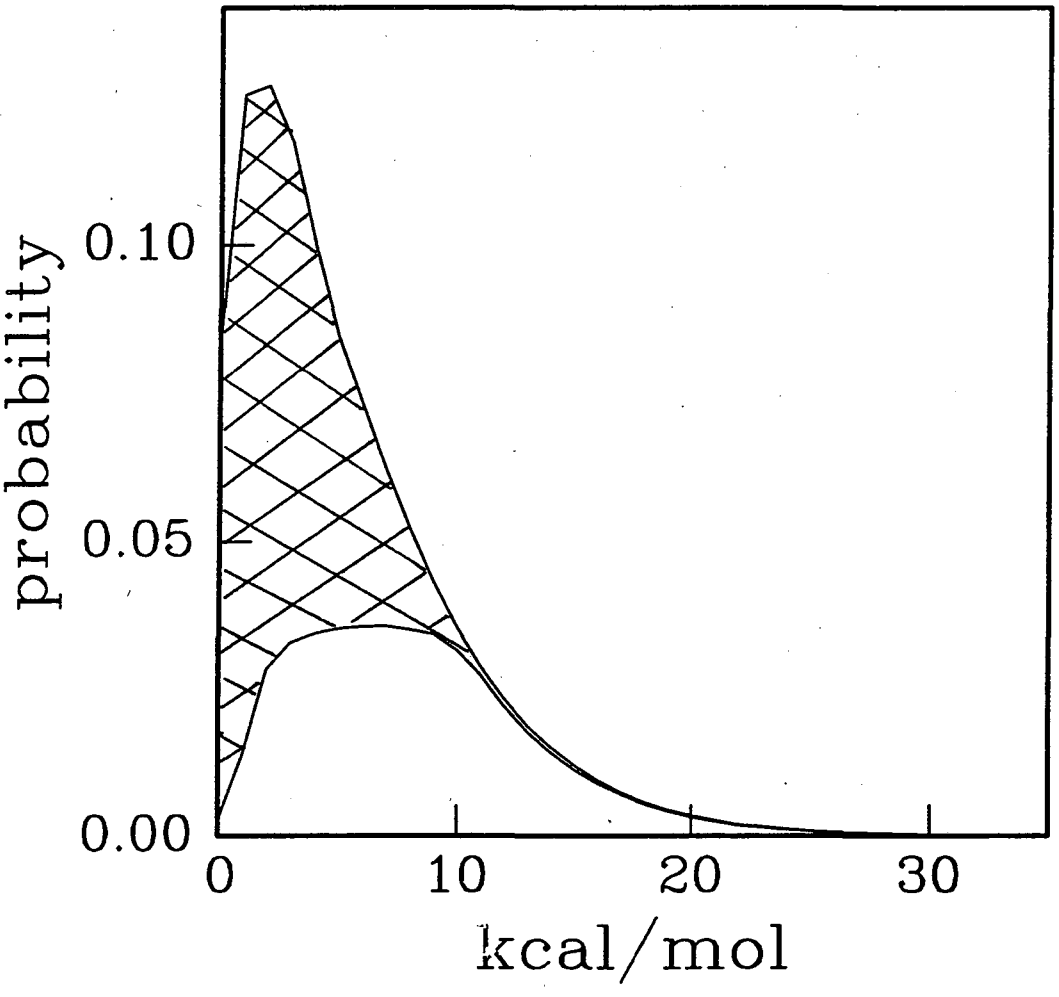

figure 7

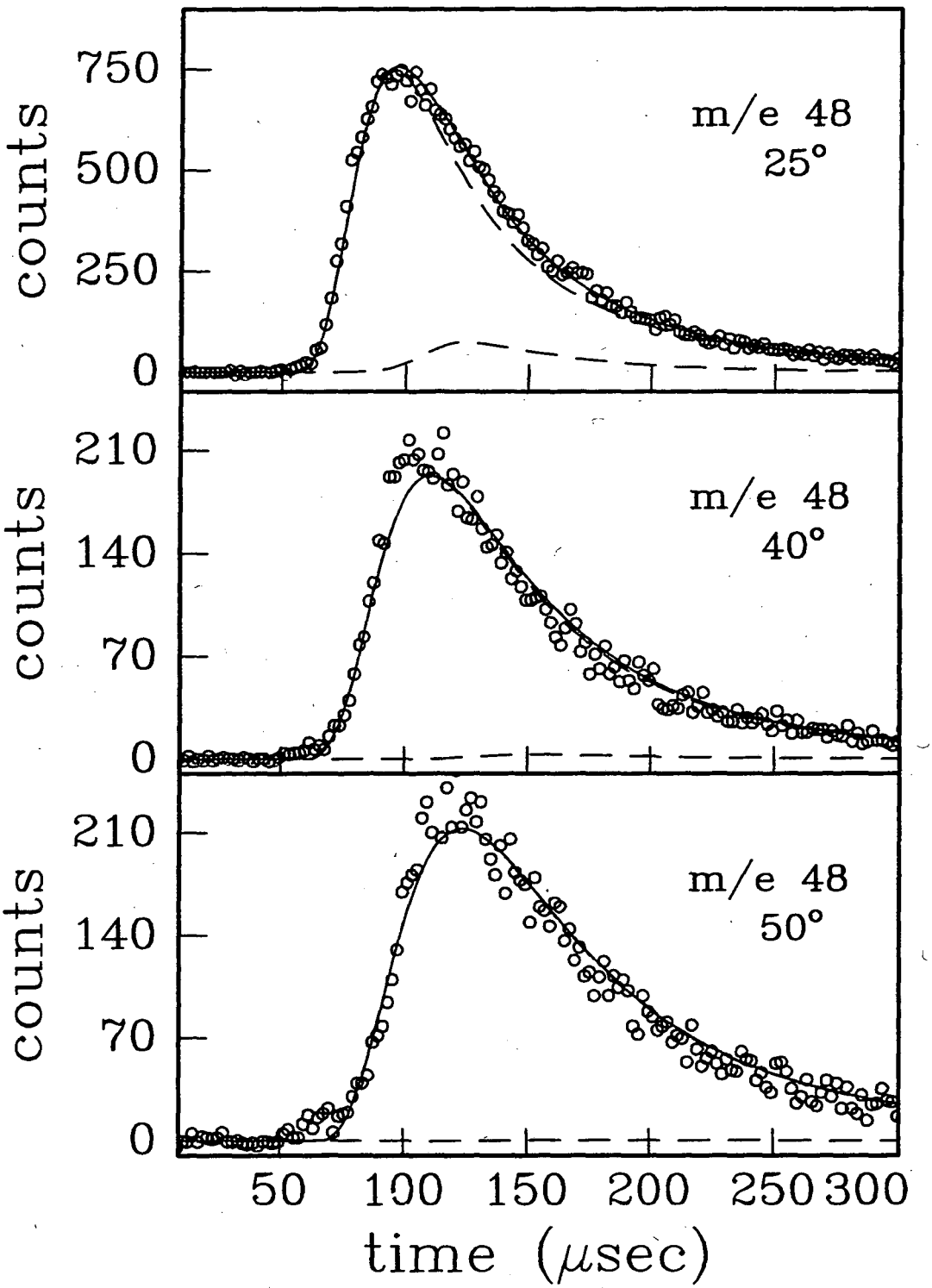
750
500
250
0
counts
m/e 48
25°
210
140
70
0
counts
m/e 48
40°
210
140
70
0
counts
m/e 48
50°
50
100
150
200
250
300
time (μsec)

figure 8

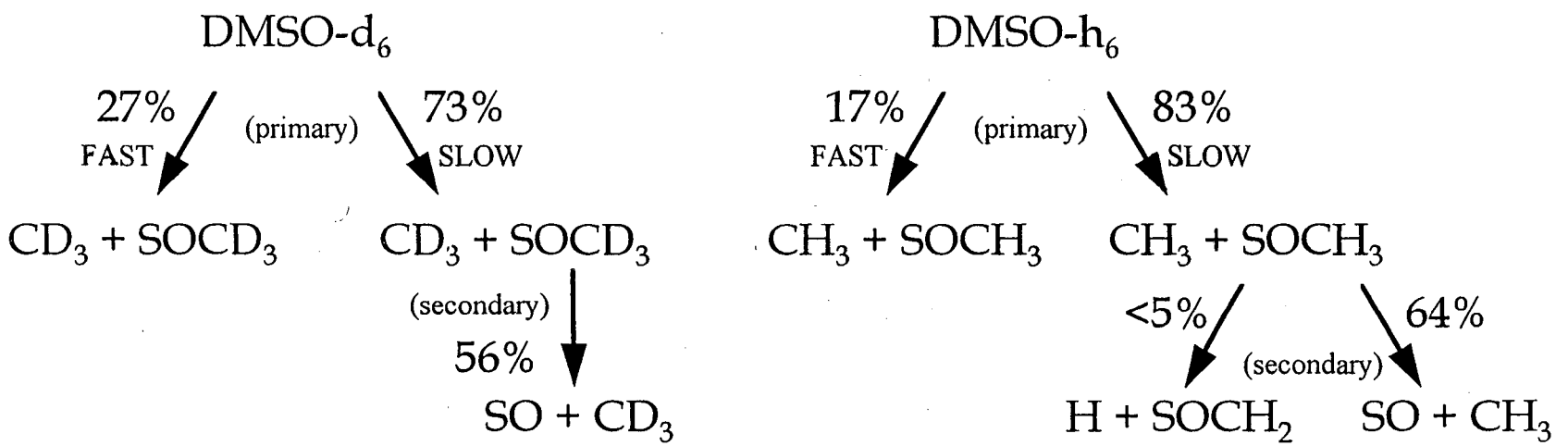
DMSO-d_6
27%
FAST
(primary)
73%
SLOW
$CD_3 + SOCD_3$
$CD_3 + SOCD_3$
(secondary)
56%
$SO + CD_3$
DMSO-h_6
17%
FAST
(primary)
83%
SLOW
$CH_3 + SOCH_3$
$CH_3 + SOCH_3$
<5%
64%
(secondary)
$H + SOCH_2$
$SO + CH_3$

figure 9

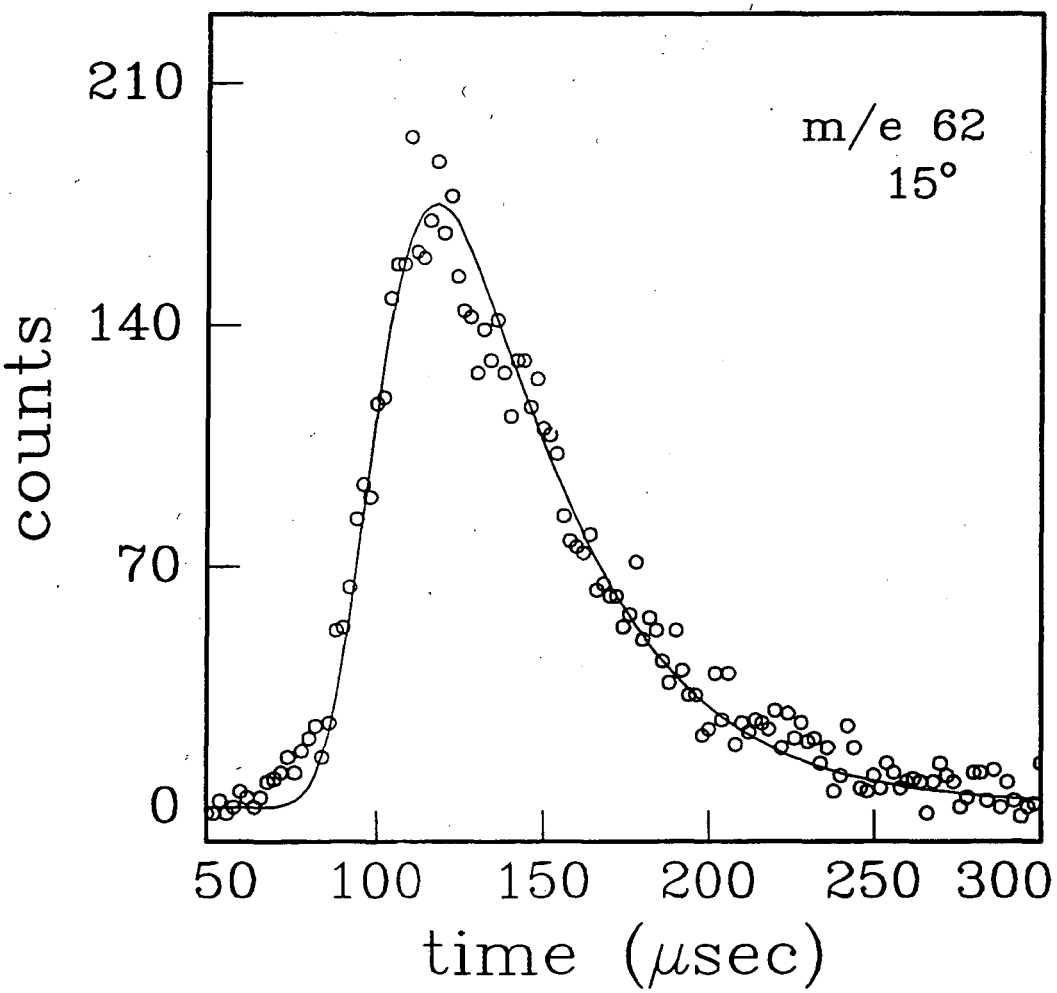

figure 10

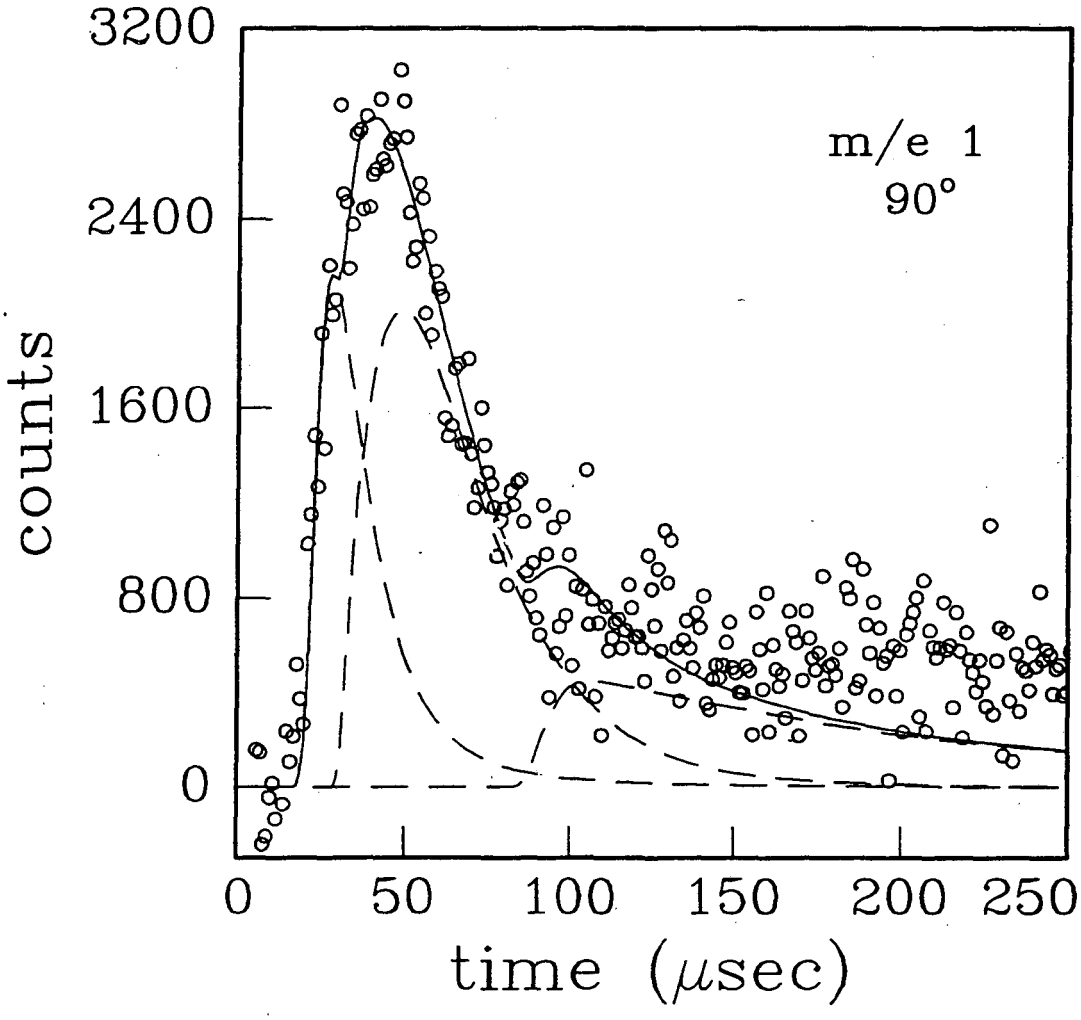
3200
2400
1600
800
0
counts
m/e 1
90°
0
50
100
150
200
250
time (μsec)

figure 11

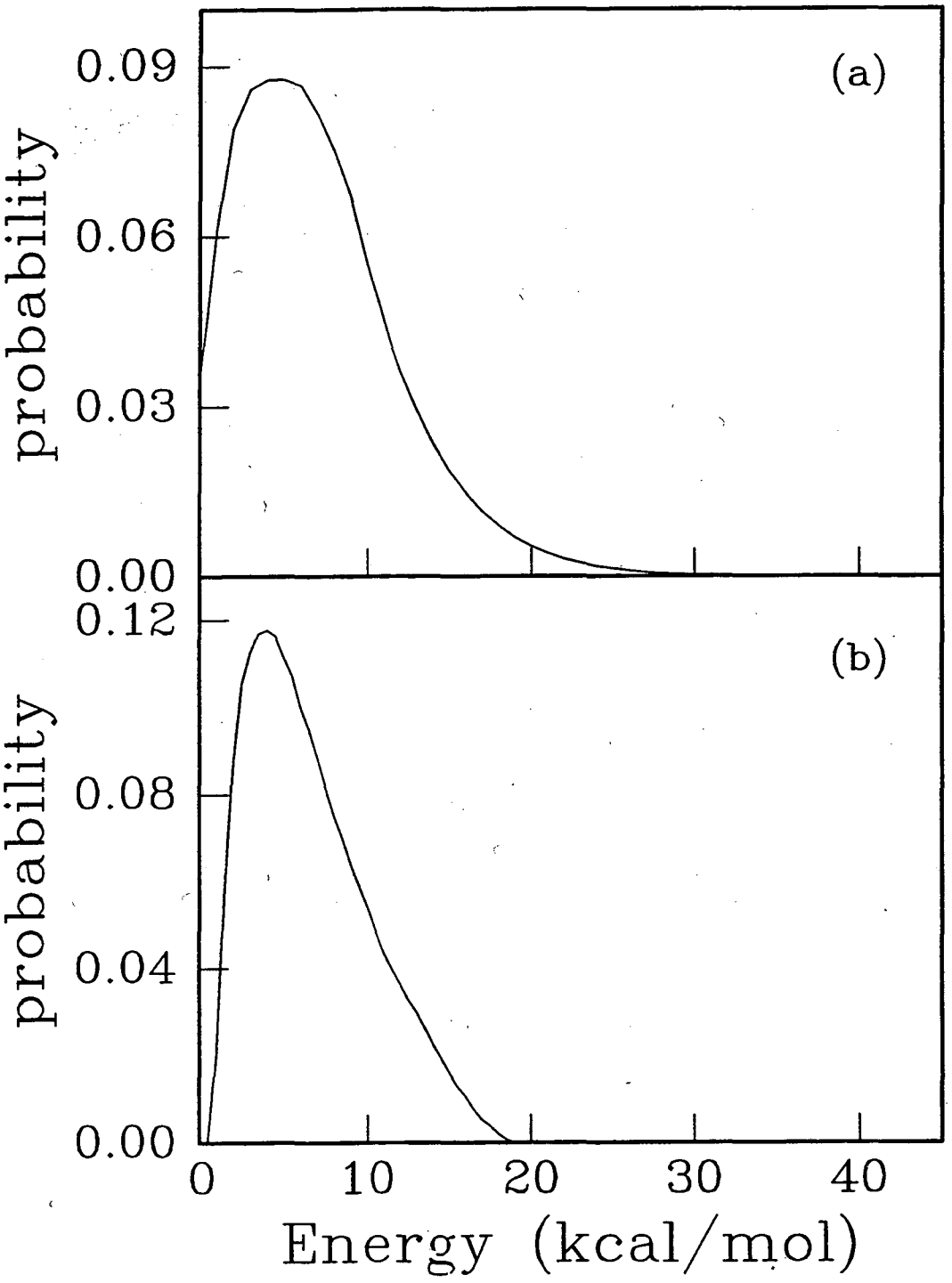
0.09
0.06
0.03
0.00
probability
(a)
0.12
0.08
0.04
0.00
probability
(b)
0
10
20
30
40
Energy (kcal/mol)

figure 12

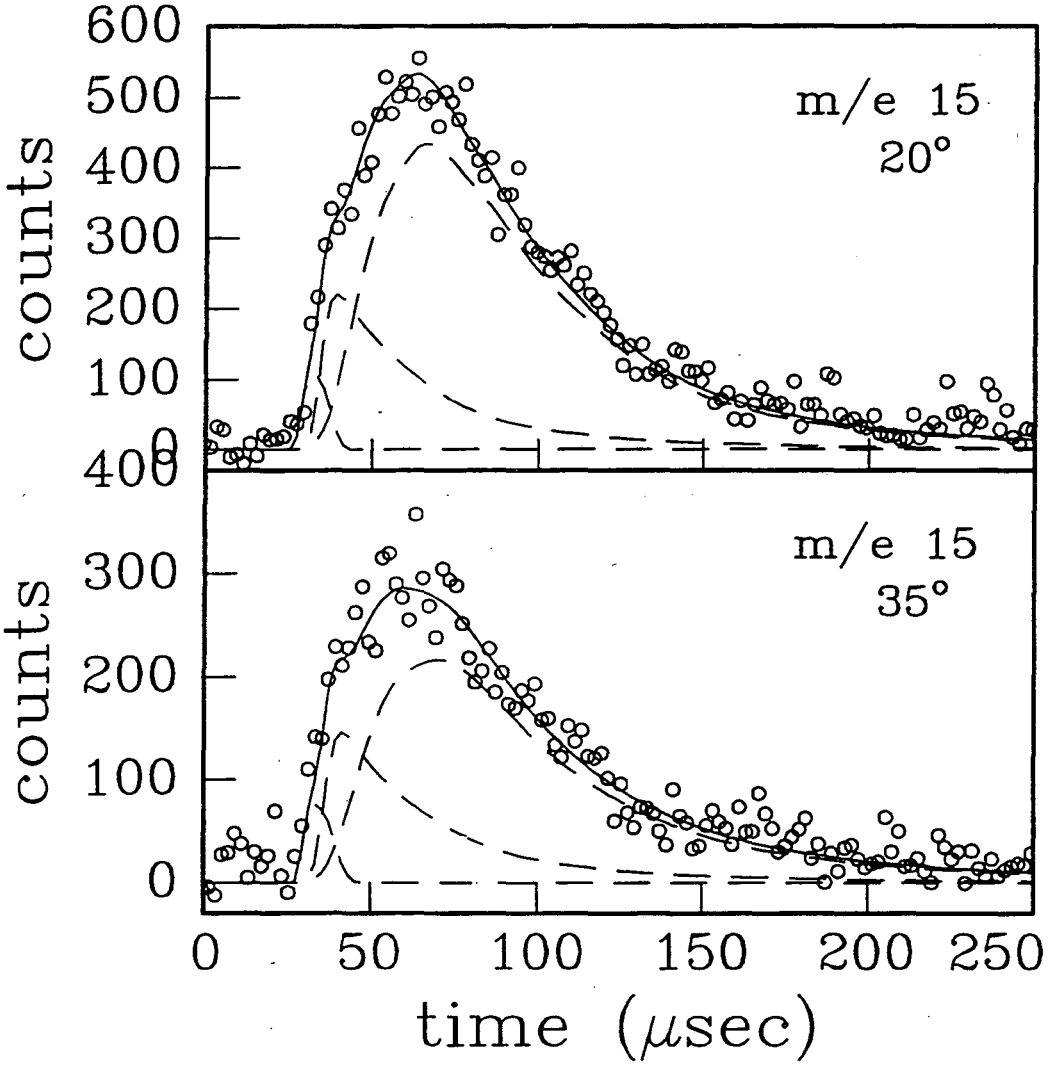
600
500
400
300
200
100
0
counts
m/e 15
20°
400
300
200
100
0
counts
m/e 15
35°
0
50
100
150
200
250
time (μsec)

figure 13

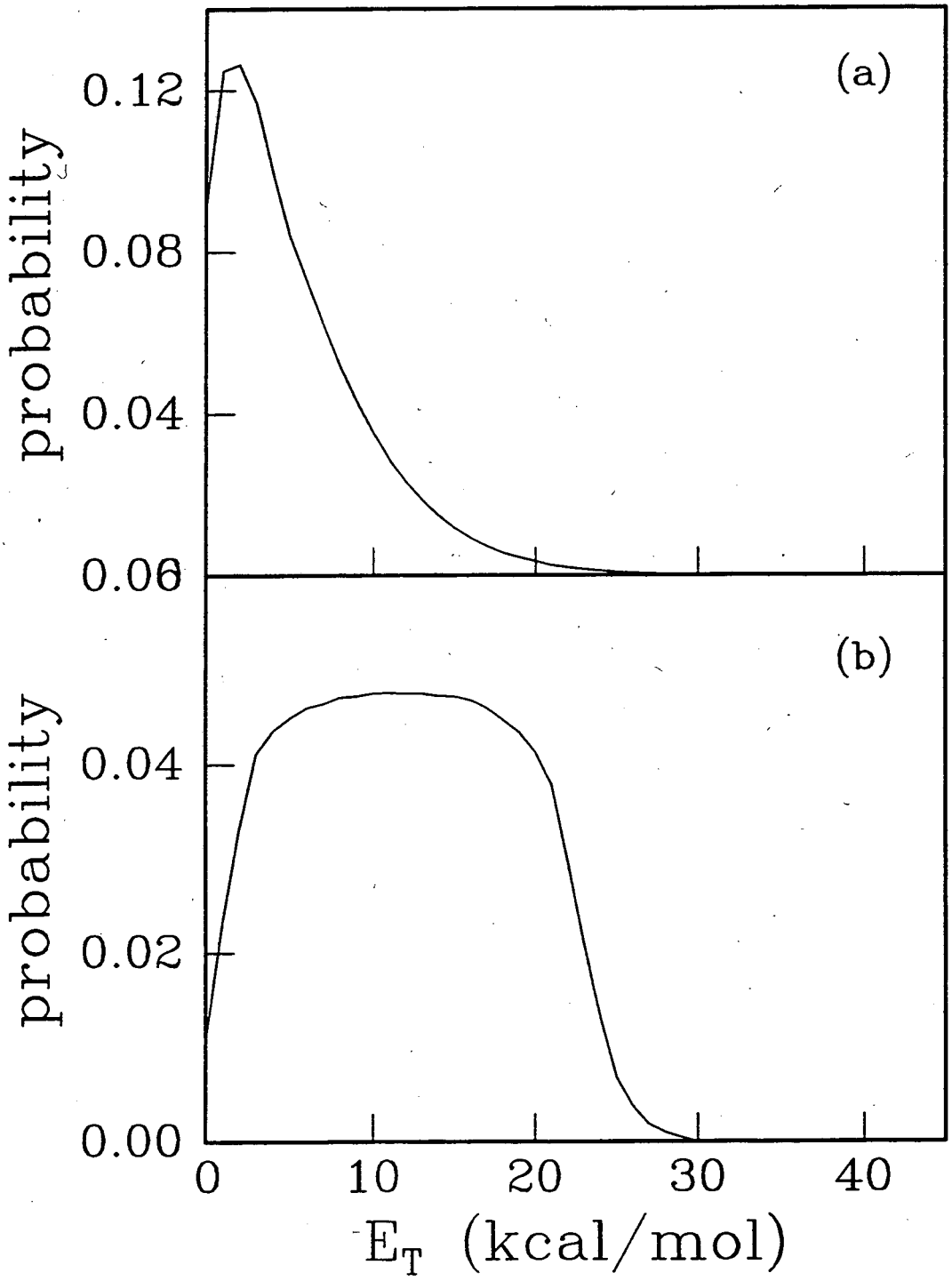
(a)
(b)
probability
probability
0.12
0.08
0.04
0.06
0.04
0.02
0.00
0
10
20
30
40
E_T (kcal/mol)

figure 14

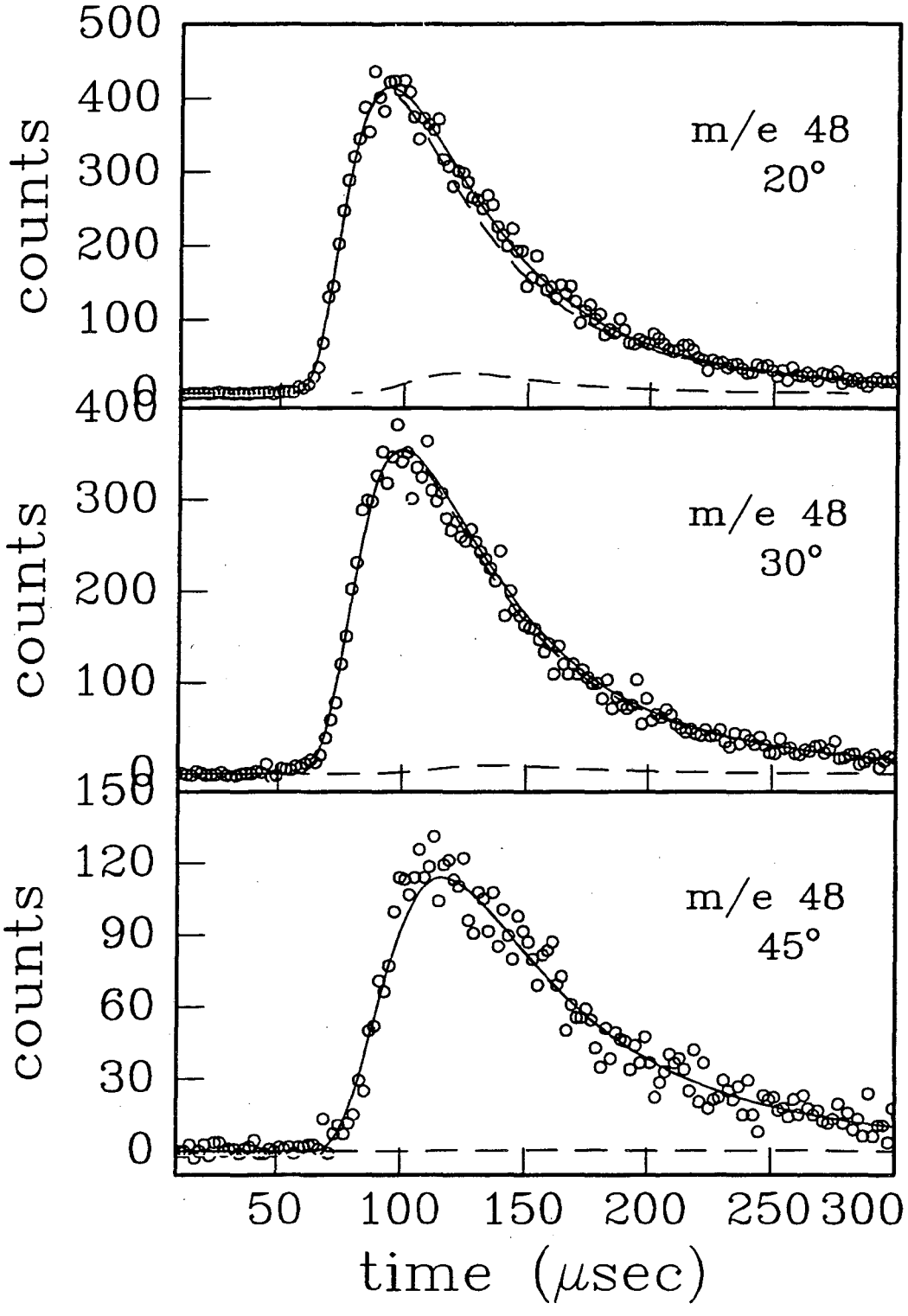
counts
500
400
300
200
100
0
m/e 48
20°
counts
400
300
200
100
0
m/e 48
30°
counts
150
120
90
60
30
0
m/e 48
45°
50
100
150
200
250
300
time (μsec)

figure 15

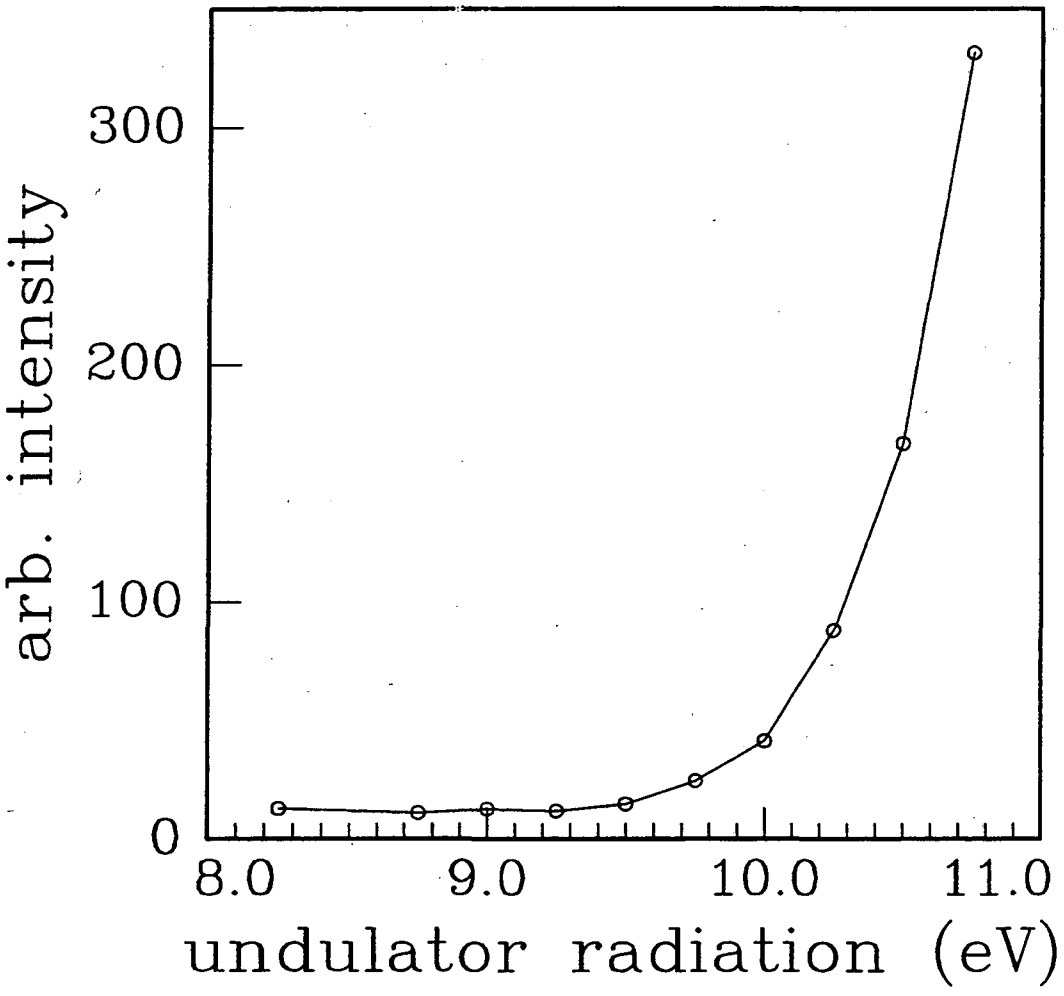
arb. intensity
300
200
100
0
8.0
9.0
10.0
11.0
undulator radiation (eV)

figure 16

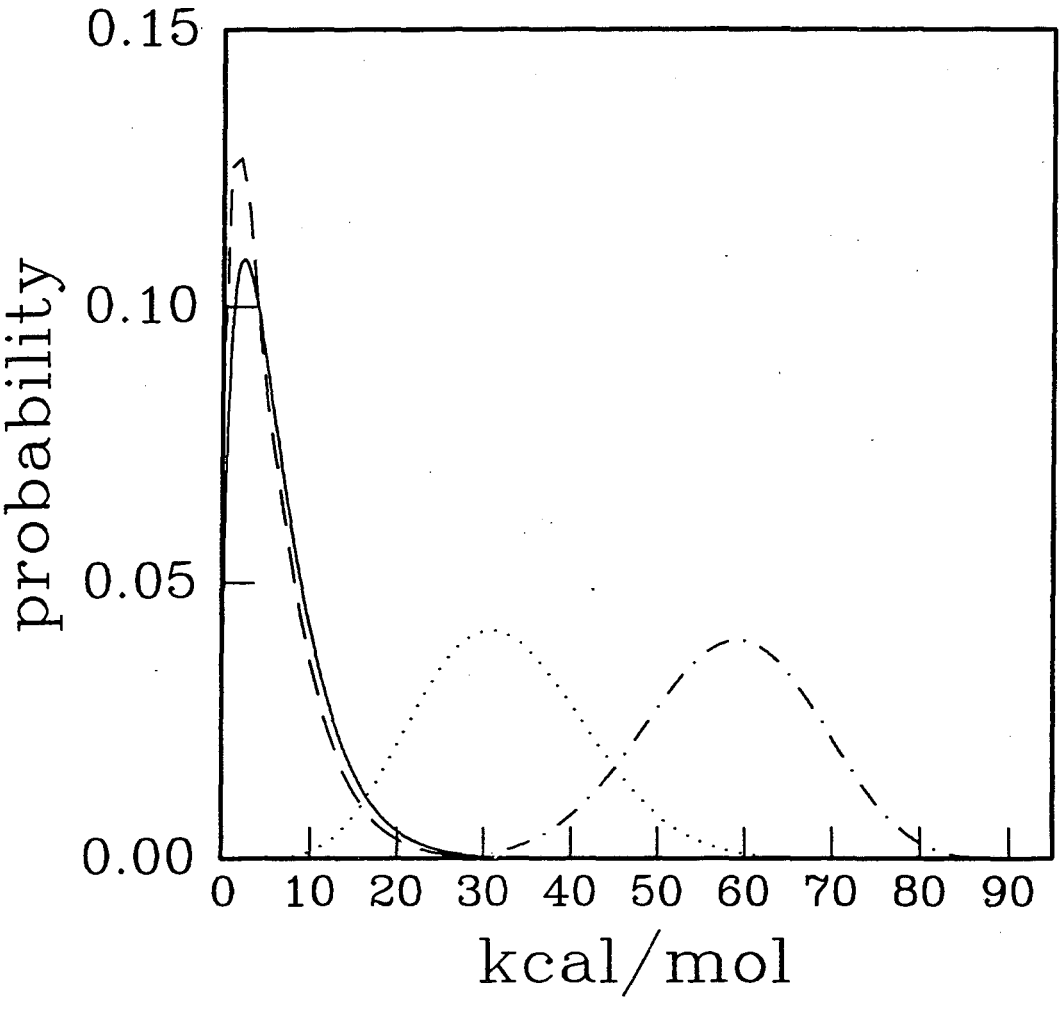

figure 17

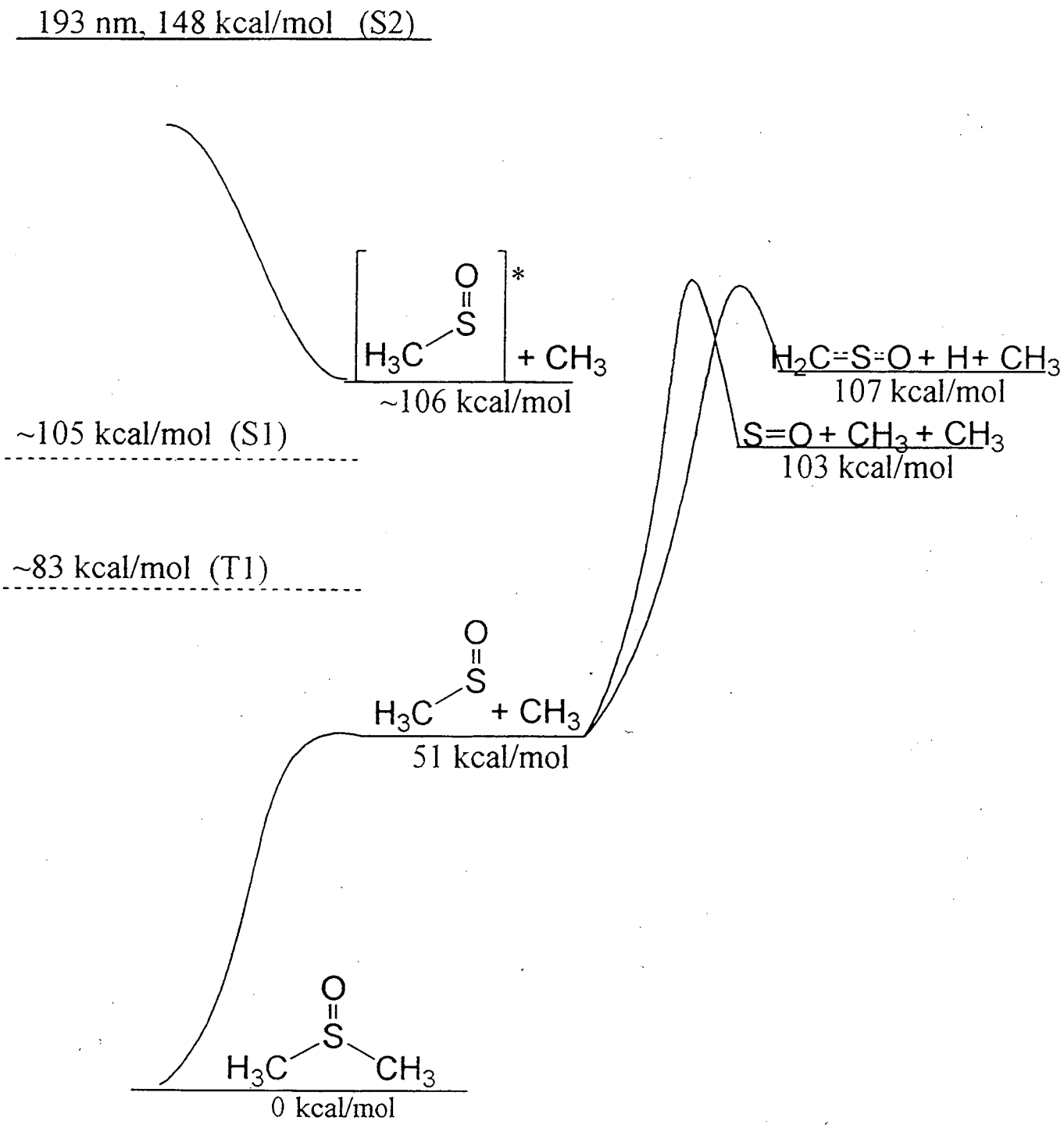
193 nm, 148 kcal/mol (S2)
~105 kcal/mol (S1)
~83 kcal/mol (T1)
~106 kcal/mol
+ CH3
H2C=S=O + H+ CH3
107 kcal/mol
S=O + CH3 + CH3
103 kcal/mol
51 kcal/mol
0 kcal/mol

ERNEST ORLANDO LAWRENCE BERKELEY NATIONAL LABORATORY
ONE CYCLOTRON ROAD | BERKELEY, CALIFORNIA 94720

Prepared for the U.S. Department of Energy under Contract No. DE-AC03-76SF00098